INTERNATIONAL ATOMIC ENERGY AGENCY
UNITED NATIONS EDUCATIONAL, SCIENTIFIC AND CULTURAL ORGANIZATION
INTERNATIONAL CENTRE FOR THEORETICAL PHYSICS
I.C.T.P., P.O. BOX 586, 34100 TRIESTE, ITALY, CABLE: CENTRATOM TRIESTE

H4.SMR/480-3

WORKSHOP ON EARTHQUAKE SOURCES
& REGIONAL LITHOSPHERIC
STRUCTURES FROM SEISMIC WAVE DATA

19 - 30 November 1990

LARGE-SCALE WAVEFORM INVERSIONS OF SURFACE WAVES FOR LATERAL HETEROGENEITY

R. SNEIDER

Dept. of Theoretical Geophysics
University of Utrecht
Utrecht, The Netherlands

JOURNAL OF GEOPHYSICAL RESEARCH. VOL. 93, NO. B10, PAGES 12,067–12,080, OCTOBER 10, 1988

Large-Scale Waveform Inversions of Surface Waves for Lateral Heterogeneity
2. Application to Surface Waves in Europe and the Mediterranean

ROEL SNIEDER

Department of Theoretical Geophysics, University of Utrecht, The Netherlands

Linear surface wave scattering theory is used to reconstruct the lateral heterogeneity under Europe and the Mediterranean using surface wave data recorded with the Network of Autonomously Recording Seismographs (NARS). The waveform inversion of the phase and the amplitude of the direct surface wave leads to a variance reduction of approximately 40% and results in phase velocity maps in the period ranges 30–40 s, 40–60 s and 60–100 s. A resolution analysis is performed in order to establish the lateral resolution of these inversions. Using the phase velocity perturbations of the three period bands, a two-layer model for the *S* velocity under Europe and the Mediterranean is constructed. The *S* velocity perturbations in the deepest layer (100–200 km) are much more pronounced than in the top layer (0–100 km), which confirms that the low-velocity zone exhibits pronounced lateral variations. In both layers the *S* velocity is low under the western Mediterranean, while the *S* velocity is high under the Scandinavian shield. In the deepest layer a high *S* velocity region extends from Greece under the Adriatic to northern Italy. Several interesting smaller features, such as the Massif Central, are reconstructed. One of the spectacular features of the reconstructed models is a sharp transition in the layer between 100 and 200 km near the Tornquist-Tesseyre zone. This would indicate that there is a sharp transition at depth between Central Europe and the East European platform. The waveform inversion of the surface wave coda leads to good waveform fits, but the reconstructed models are chaotic. This is due both to a lack of sufficient data for a good imaging of the surface wave energy on the heterogeneities and to an appreciable noise component in the surface wave coda.

INTRODUCTION

One of the main tasks of modern seismology is to map the lateral heterogeneity in the Earth. Low-order spectral models of lateral heterogeneity have been constructed using *P* wave delay times [*Dziewonski*, 1984], surface wave dispersion data [*Nataf et al.*, 1986], or surface waveforms [*Woodhouse and Dziewonski*, 1984; *Tanimoto*, 1987]. These studies produced extremely smooth Earth models because of the low-order expansion of the heterogeneity in spherical harmonics. However, recent large-scale tomographic inversions of *P* wave delay times have shown that lateral heterogeneity exists down to depths of at least 500 km on a horizontal scale of a few hundred kilometers [*Spakman*, 1986*a*,*b*].

Lateral variations in the *P* velocity on this scale can be analyzed accurately using delay time tomography. In principle, tomographic inversions could also be applied to *S* wave delay times. In practice, this is not so simple because the presence of the low-velocity layer renders the *S* wave tomography problem highly nonlinear. In fact, it is shown by *Chapman* [1987] that the tomographic inversion problem is illposed if a low-velocity layer is present. The fact that the low-velocity layer exhibits strong lateral variations [*York and Helmberger*, 1973; *Souriau*, 1981; *Paulssen*, 1987] poses an additional complication.

One could use surface wave data instead because Love waves and Rayleigh waves are strongly influenced by the *S* velocity. However, fundamental mode surface wave data (which are most easily measured and identified) that penetrate as deep as 200 km, have a horizontal wavelength of the order of 300 km. This means that lateral heterogeneities on a scale of a few hundred kilometers are no longer smooth on a scale of a wavelength of these waves. Therefore ray theory, which forms the basis of all dispersion measurements, cannot be used in that case. Up to this point, this fact has been consequently ignored.

The breakdown of ray theory means that scattering and multipathing effects can be important. In the companion paper [*Snieder*, this issue; (hereafter referred to as "paper 1")], linear surface wave scattering theory is presented. It is shown in paper 1 how this theory can be used to map the lateral variations of the *S* velocity in the Earth. With this method, complete waveforms of surface wave data can be inverted, so that not only the phase but also the amplitude can be used for inversion. Unfortunately, there is at this point only linear theory for surface wave scattering in three dimensions [*Snieder*, 1986*a*,*b*; *Snieder and Nolet*, 1987; *Snieder and Romanowicz*, 1988; *Romanowicz and Snieder*, 1988] which limits the applicability of this method. Large-scale inversion of both the phase and the amplitude of surface wave data has also been performed by *Yomogida and Aki* [1987], who applied a scattering formalism to the Rytov field of surface waves. However, their method is based on the assumption that surface waves satisfy the two-dimensional wave equation, which has never been shown (and which is probably not true).

In this paper, large-scale waveform inversions using linear scattering theory, as presented in paper 1, are applied to surface wave data recorded with the Network of Autonomously Recording Seismographs (NARS) [*Dost et al.*, 1984; *Nolet et al.*, 1986] for events in southern Europe. The inversions with linear scattering theory, which will be called the "Born inversion," are applied both to the surface wave coda and to the direct surface wave. Details of the inversion method with numerical examples are shown in paper 1.

The Born inversion is first applied to the surface wave coda. To this end the nature of the surface wave coda is investigated in section 2, and the conditions for the validity of the Born approximation for the surface wave coda are established. In inversions of the complete waveform, parameters like the source mechanism, station amplification, etc., should be specified correctly. The procedures that are followed in this study are reported in section 3. As shown in paper 1, it may be

Paper number 7B6094.
0148-0227/88/007B-6094$05.00

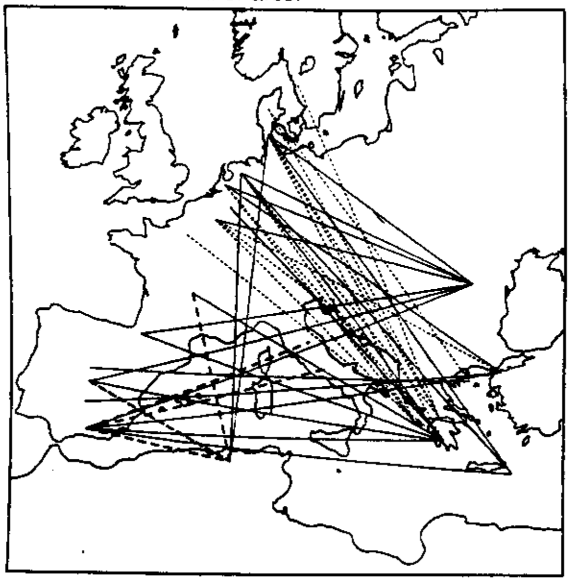

Fig. 1. Source-receiver minor arcs for the seismograms used in the inversions. The dashed minor arcs correspond to the seismograms used in the computation of the spectra for the western Mediterranean, while the minor arcs used for the spectra for the paths in Europe are dotted. The seismograms for all minor arcs (dashed, dotted, and solid) are used in the waveform inversions.

advantageous to perform a nonlinear inversion first for a smooth reference model in order to render the problem more linear. The results of this nonlinear inversion are shown in section 4. Section 5 features waveform inversions of the surface wave coda, while in section 6 the Born inversions of the direct wave are shown. The reliability of these results is investigated in section 7, where a resolution analysis is presented. A two-layer model of the S velocity under Europe and the Mediterranean is finally presented in section 8.

2. NATURE OF THE SURFACE WAVE CODA

Before proceeding with the inversion, it is instructive to study the surface wave coda in some more detail. In this study, surface wave data recorded by the NARS array [*Dost et al.*, 1984; *Nolet et al.*, 1986] are used for shallow events around the Mediterranean and a deeper event in Rumania. Figure 1 shows the source receiver minor arcs for the seismograms used in this study. Because the inversion is linear, it is important to establish first the conditions for the validity of the Born approximation for the surface wave coda.

In Figure 2 a seismogram is shown for an event in Algeria recorded at station NE03 in Denmark, low passed at several different periods. For the seismogram low passed at 16 s, the coda has approximately the same strength as the direct wave. This means that the Born approximation cannot be used to describe the surface wave coda at these periods. However, for periods larger than 20 s the coda is much weaker than the direct wave, which justifies the Born approximation for these periods. Low passed seismograms recorded in the same station for a Greek event at approximately the same depth are shown in Figure 3. For this event in the seismogram low passed at 25 s, there is still an appreciable secondary wave train (around 700 s) just after the arrival of the direct wave, and the Born approximation for the surface wave coda is therefore only justified for periods larger than 30 s. (This is confirmed later by Figure 4*b*.) Therefore only periods larger than 30 s have been used in the inversions presented in this paper. It is verified that for all recorded seismograms low pass filtering at 30 s leads to a coda level which is low enough to justify the Born approximation.

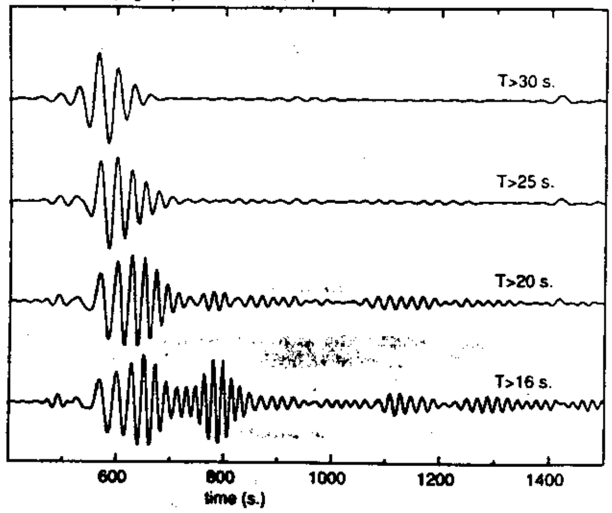

Fig. 2. Low passed seismograms for an Algerian event recorded in NE03 (Denmark).

This condition for the validity of the Born approximation may be overconservative. In a field experiment, surface waves reflected from a concrete dam on a tidal flat have been used successfully to reconstruct the location of this dam using Born inversion [*Snieder*, 1987*a*]. Due to the very large contrast posed by this dam, the direct surface wave and the reflected surface wave had approximately the same strength, and Born inversion was strictly not justified. Nevertheless, an accurate reconstruction of the location of this dam was achieved. The reason for this discrepancy is that the geometry of the heterogeneity precluded multiple scattering. In such a situation, linear inversion gives at least qualitatively good results.

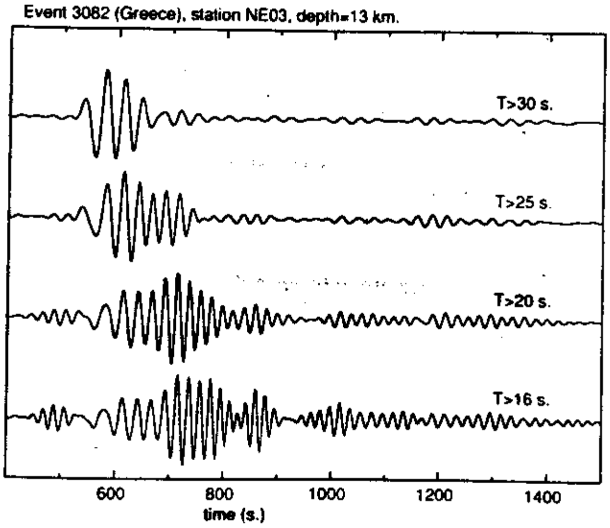

Fig. 3. Low passed seismograms for a Greek event recorded in NE03 (Denmark).

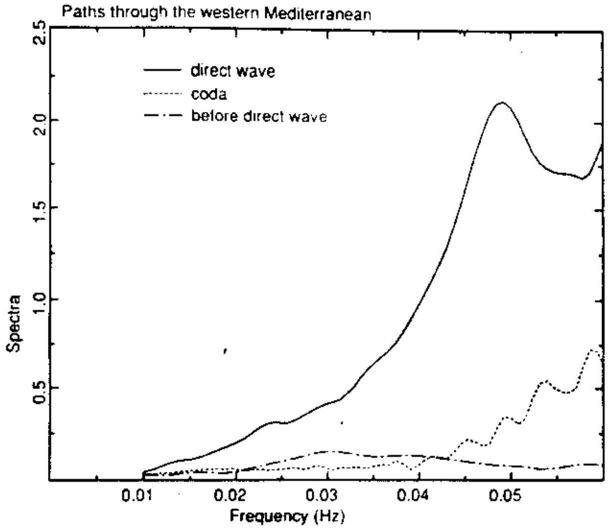

Fig. 4a. Spectra of the direct wave, surface wave coda, and background noise for wave paths through the western Mediterranean.

The examples shown in the Figures 2 and 3 show that the coda level is very different for the different wave paths. This is verified by dividing the seismograms in two groups. One group consists of seismograms for with wave paths through the western Mediterranean (the dashed lines in Figure 1), while the other group is for the wave paths through eastern and central Europe (the dotted lines in Figure 1). For each group the spectrum of the direct surface wave is determined, as well as the spectum of the coda (defined by group velocities between 1.6 and 2.9 km/s), and the spectrum of the signal before the arrival of the direct wave. The spectrum of the signal before the arrival of the direct wave is considered to give an estimate of the background noise level. From an academic point of view this is acceptable because body waves and higher-mode surface waves are noise for our purposes. On the other hand, this procedure may give an overestimate of the background noise.

The spectra for the paths through the western Mediterranean are shown in Figure 4*a*. Note that the average coda level is much weaker than the strength of the direct surface wave, even for periods as short as 16 s (0.06 Hz). For periods larger than 25 s (0.04 Hz) the noise level has about the same strength as the coda level. The means that inversions using the surface wave coda for these periods can only give meaningful results if there is an abundance of data, which leads to a system of linear equations which is sufficiently overdetermined to average out the contaminating influence of noise. For the wave paths through eastern and central Europe (Figure 4*b*) the situation is different. For all frequencies the coda level lies above the noise level, although for periods longer than 50 s (0.02 Hz) this difference is marginal. For these seismograms the coda energy increases rapidly as a function of frequency; for periods shorter than 22 s (0.045 Hz) the coda spectrum is even higher than the spectrum of the direct wave. This means that there is only a relatively narrow frequency band where the Born approximation is valid and where the coda stands out well above the noise level.

The fact that the coda level for the paths through eastern and central Europe increases more rapidly as a function of frequency than for the paths through the western Mediterranean has implications for the depth of the heterogeneities that generate the coda. In order to quantify this notion a normalized coda level can be defined by subtracting a constant noise level from the coda spectrum and by division by the spectrum of the direct wave. This normalized coda level is approximately equal to the interaction coefficients, see equations (1) and (5) of paper 1. (One should be a bit careful with this identification because an organized distribution of scatterers leads to extra frequency dependent factors; see *Snieder* [1986*a*] for an example of scattering of surface waves by a quarter space.)

The normalized coda levels are compared with the interaction terms for different heterogeneities the Figures 5*a* and 5*b*. (In this example the absolute value of the interaction terms is averaged over all scattering angles.) These inhomogeneities have a constant relative shear wave velocity perturbation down to the indicated depth, while the density is unperturbed; furthermore, $\delta\lambda=\delta\mu$. For the wave paths through eastern and central Europe these curves in Figure 5*b* can only be compared with the interaction terms for periods longer than 30 s, because the condition of linearity breaks down for shorter periods. All shown heterogeneities fit the normalized coda level within the accuracy of the measurements. Also, it follows from Figures 1*a* and *b* of paper 1 that these heterogeneities have approximately the same radiation pattern. This means that for these wave paths it is virtually impossible to determine the depth of the heterogeneity from the surface wave coda. For the paths through the western Mediterranean this situation is different because it can be seen from Figure 5*a* that a shallow heterogeneity (or topography) fits the normalized coda spectrum better than a deeper inhomogeneity. This is an indication that the lateral heterogeneity in eastern and central Europe is present at greater depths than in the western Mediterranean.

3. PROCEDURES FOR THE INVERSION OF SURFACE WAVE SEISMOGRAMS

In order to perform waveform fits of surface wave data, several parameters and procedures need to be specified. All inversions presented in this paper have been performed with the model shown in Figure 6. This model is equal to the M7 model of *Nolet* [1977], except that the *S* velocity in the top 170 km is 2% lower than in the M7 model. This compensates for the fact that the M7 model is for the Scandinavian shield which has an anomalously high *S* velocity. The anelastic damping of the PREM model

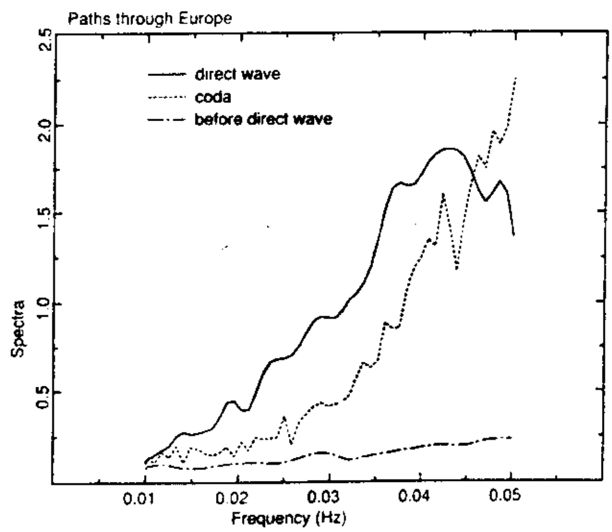

Fig. 4*b*. Spectra of the direct wave, surface wave coda, and background noise for wave paths through eastern and central Europe.

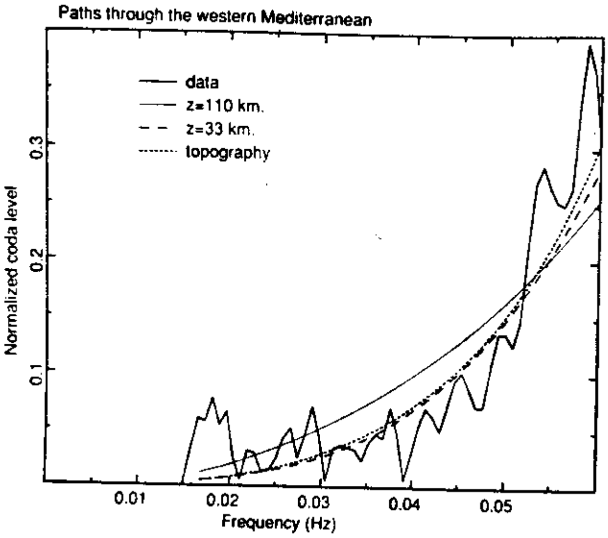

Fig. 5*a*. Normalized coda level for the wave paths through the western Mediterranean and the (normalized) integrated radiation for different inhomogeneities as defined in section 3.

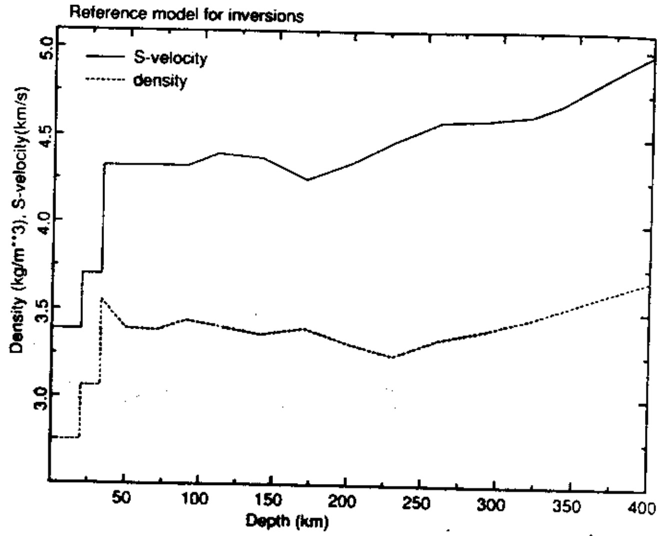

Fig. 6. Starting model for the inversions.

[*Dziewonski and Anderson*, 1981] is assumed; this damping is not varied in the inversions.

For the source mechanisms and the event location and depth, the centroid moment tensor solutions, as reported in the International Seismological Centre bulletins, are used whenever available. For the remaining events the source parameters from the Preliminary Determination of Epicenters bulletins are used. For the Rumania event the source mechanism as determined from GEOSCOPE data (B. Romanowicz, personal communication, 1986) is employed. No inversion for the source mechanism is performed because the NARS stations provide only a limited azimuthal coverage, which means that the source mechanisms are poorly constrained by the data. The source strength is usually rather inaccurate; this parameter is determined by fitting the envelopes of the synthetics to the data envelopes. The events used in this study are, in general, rather weak ($ms \approx 5$-6), so that the reported source mechanisms are not always reliable. All seismograms with a strong difference in wave shape between the data and the (initial) synthetics have not been used in the inversion. Surface wave recordings that triggered on the surface wave have also been discarded.

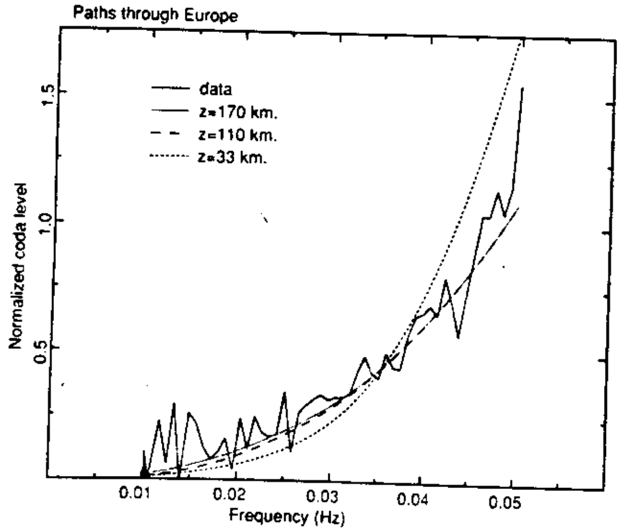

Fig. 5*b*. Normalized coda level for the wave paths through eastern and central Europe and the (normalized) integrated radiation for different inhomogeneities as defined in section 3.

The station magnifications are not included in the inversions presented here. The station magnification includes not only the instrumental magnification but also the magnification effects of the local environment of the station. As a check, the inversions presented here have also been performed with a simultaneous inversion for the station amplifications. Even though this produced station magnifications as large as 10%, the result in the models for lateral heterogeneity was minimal.

In paper 1, the waveform inversion is formulated as the least squares solution of a large matrix equation. The rows and columns of this matrix can be scaled at will [*Van der Sluis and Van der Vorst*, 1987]. It has been shown by *Tanimoto* [1987] that it is important that each seismogram gets more or less the same weight in the inversion. Similarly, the different frequency components within each seismogram should have a comparable weight. For the shallow events used here, the low frequencies are not excited very well. In order to compensate for this, data and synthetics are scaled in the frequency domain with a factor $1/\omega$. In the inversions for the surface wave coda, a scaling with $M_o/\sqrt{\sin\Delta}$ is applied, where M_o is the strength of the moment tensor and Δ is the epicentral distance. This factor corrects for the different strengths and geometrical spreading factors of the different events. In the inversion for the direct wave the seismograms are scaled in such a way that maximum amplitude in the time domain is equalized.

Last, in the Born inversions both for the coda and the direct wave, each seismogram is scaled with a factor $1/\sqrt{1+E/\langle E\rangle}$. In this expression, E is the energy of the data residual of the seismogram under consideration, while $\langle E\rangle$ denotes the average of this quantity for all seismograms. This weight factor ensures that the seismograms with appreciable misfits get more or less the same weight in the inversion, so that the contaminating influence of outliers is reduced. In the meantime, seismograms with a good initial fit have a low weight in the inversion; this prevents a small amount of spurious noise in these seismograms getting an excessive weight in the inversion.

4. NONLINEAR INVERSION OF THE DIRECT WAVE

As mentioned in paper 1, it is advantageous to perform a nonlinear inversion of the direct wave first because this renders the Born inversion more linear. For this inversion the procedures described in paper 1 are used for determining the phase velocity perturbation of a smooth reference model. In this inversion the phase velocity is determined on a rectangular grid of 12×12 points in the domain shown in Figure 1 and is interpolated at intermediate locations using bicubic splines. The relative phase velocity perturbation $\delta c/c$ is assumed to be constant in the period bands 30–40 s, 40–60 s, and 60–100 s.

In Figure 7*a* the phase velocity perturbation for periods between 60 s and 100 s is shown for the unconstrained case, i.e., $\gamma=0$ in equation (21) of paper 1. Note that the phase velocity perturbations are not confined to the vicinity of the source receiver paths. This is an artifact of the bicubic spline parameterization, which has an oscillatory nature near places where the interpolated function changes rapidly. These artifacts can be removed by switching on the regularization parameter γ in expression (21) of paper 1. The constrained solution ($\gamma>0$) is shown in Figure 7*b*. This regularization goes at the expense of the waveform fit, and it is subjective how much regularization one wants to impose on these solution. However, in this study the nonlinear inversion for a smooth reference model is only the first step in the complete waveform inversion, so that there is no need to obtain the maximum information from this nonlinear inversion. For periods larger than 30 s the resulting reference models for the employed value of γ (see, for example, Figure 7*b*) produce a waveform fit which is sufficiently good to warrant a linear inversion for the remaining data residual. (This means that the phase shift between the data and synthetics is at the most 45°, and that the amplitude mismatch is not larger than 30%.) These reference models for the phase velocity perturbations are used in the subsequent Born inversions. Waveform fits of the nonlinear inversion are presented in section 6.

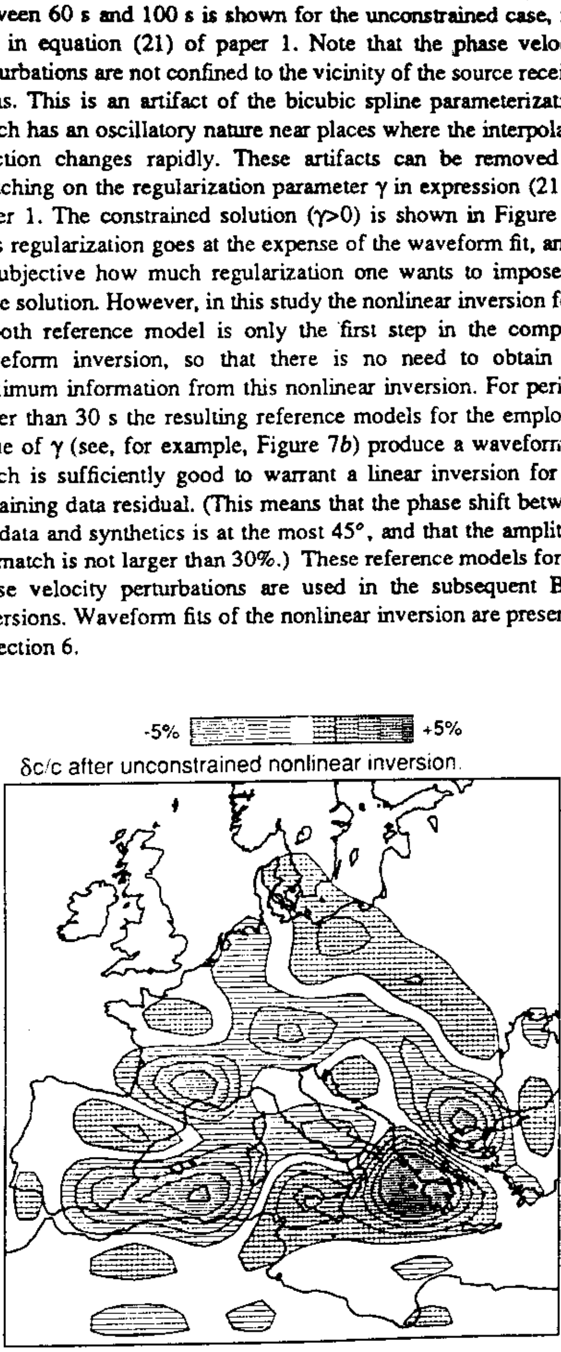

Fig. 7*a*. Relative phase velocity perturbation ($\delta c/c$) for periods between 60 and 100 s determined from unconstrained nonlinear waveform fitting ($\gamma=0$).

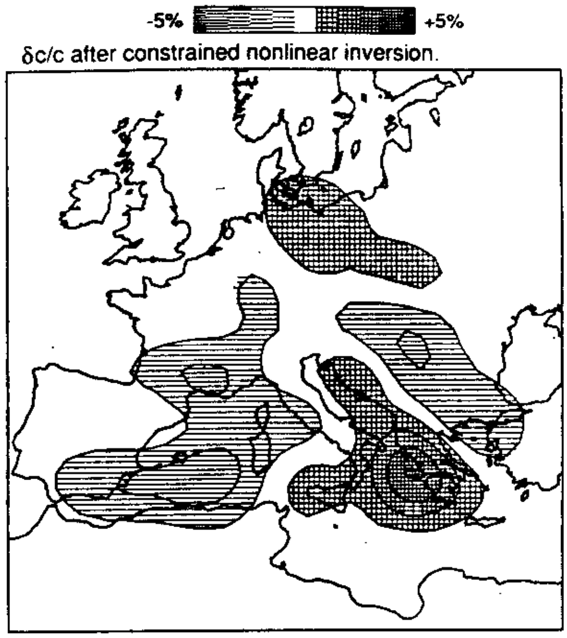

Fig. 7*b*. Relative phase velocity perturbation ($\delta c/c$) for periods between 60 and 100 s determined from constrained nonlinear waveform fitting ($\gamma>0$.).

5. BORN INVERSION OF THE SURFACE WAVE CODA

The Born inversion can be applied both for inversion of the direct surface wave, as well as for the coda. In this section the waveform inversion of the surface wave coda is discussed. The surface wave coda is extracted from the full seismogram with a time window that allows group velocities between 1.74 and 2.90 km/s. At both ends this window is tapered with a cosine taper over a length of 100 s.

In this inversion the depth dependence of the heterogeneity is prescribed to consist of a constant relative *S* velocity perturbation $\delta\beta/\beta$ down to a depth of 170 km, while the density is unperturbed. The perturbations on the Lamé parameters are equal. In the inversion a model of 100×100 cells is determined (with a cell size of 35×35 km^2), so that 10,000 unknowns are determined in the inversion. The 42 seismograms produce 2520 data points, where the real and imaginary parts of each spectral component are counted as independent variables. This means that the resulting system of linear equations is underdetermined. Increasing the cell size has the disadvantage that the scattering integral (5) of paper 1 is not discretized accurately. Imposing a smoothness constraint also is no option, since scattered surface waves are most sensitive to abrupt lateral changes of the heterogeneity. As argued in section 2, it is difficult to obtain a good depth resolution for this kind of inversion. This, and the consideration that for a fixed depth dependence of the heterogeneity the resulting system of linear equation is already underdetermined, makes it unjustifiable to perform an inversion with more degrees of freedom with respect to the depth dependence of the heterogeneity.

The result of the Born inversion of the surface wave coda for periods between 30 and 100 s is shown in Figure 8. For this inversion, three iterations have been performed; according to the results of paper 1 this is sufficient to image the heterogeneity. The reconstructed model has a messy appearance and is dominated by ellipsoidal structures. These structures are reminiscent of the "smiles" that occur in improperly migrated sections in exploration

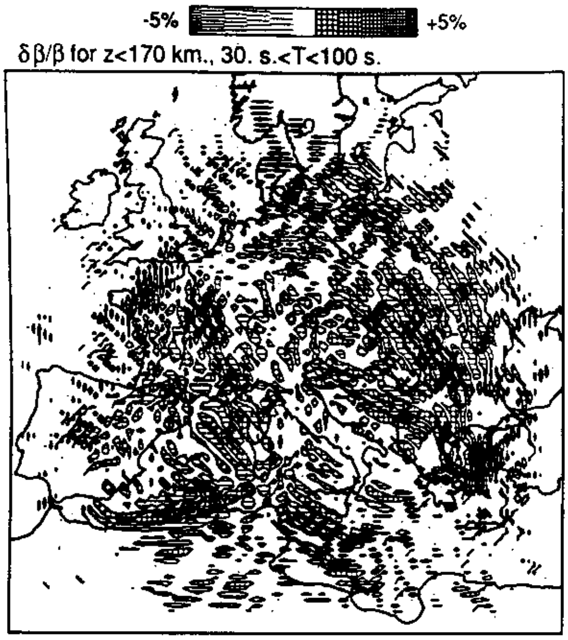

Fig. 8. Relative *S* velocity perturbation (δβ/β) from the inversion of the surface wave coda. The heterogeneity extends down to a depth of 170 km.

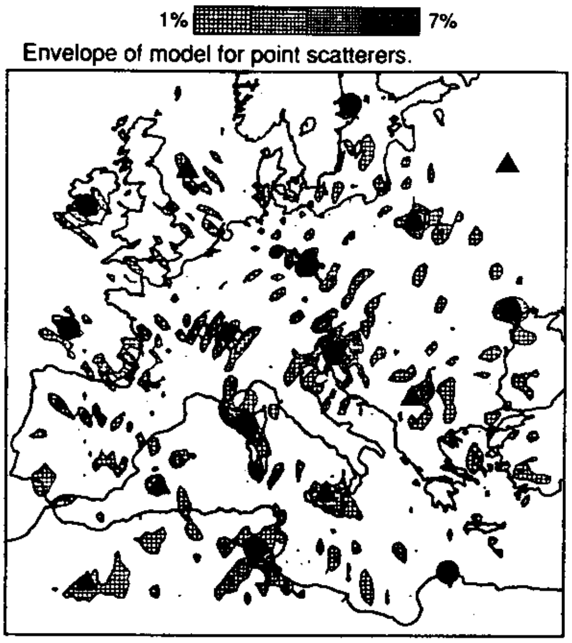

Fig. 10. Filtered envelope of the model determined from a waveform inversion of synthetics computed for positive (circles) and negative (triangles) point scatterers with δβ/β constant down to a depth of 170 km.

seismics [*Berkhout*, 1984]. Note the oscillatory nature of the solution, which is a consequence of the fact that this image is reconstructed essentially with a correlation method (paper 1). It can be seen in Figure 1 that the majority of the paths in central Europe runs in the southeast-northwest direction. The ellipsoidal structures in eastern Europe and between Sicily and France are centered around these paths. This means that just as in the synthetic example of section 8 of paper 1, the shape of these ellipsoidal stripes does not necessarily coincide with the locations of the scatterers and that some smearing of the true inhomogeneity along these stripes (smiles) has taken place in the inversion. More data, and especially more crossing paths are needed to obtain a better resolution along these ellipsoidal stripes. The direction of these ellipsoidal stripes is thus determined by the geometry of the events and the stations; it does not necessarily reflect the structure of the inhomogeneity.

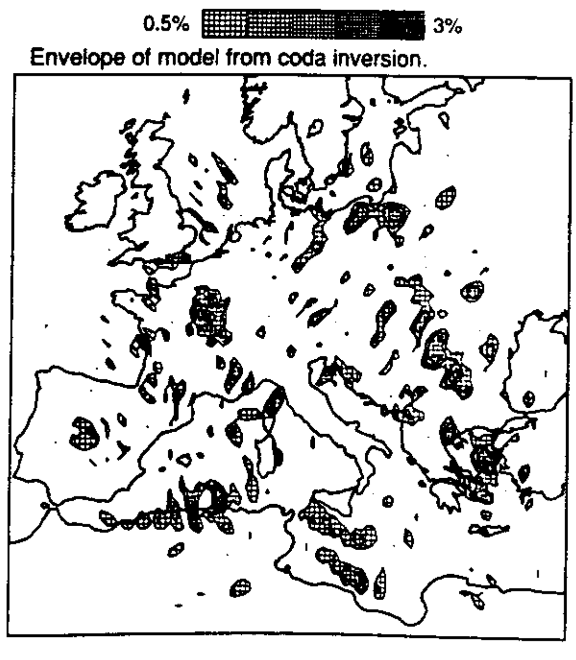

Fig. 9. Filtered envelope of the model in Figure 8.

This directivity of the oscillations in the reconstructed model can be removed by computing the two-dimensional spatial envelope of the solution in Figure 8. Subtracting a smoothed version of this envelope from the envelope itself enhances the contrasts in the final solution. The result of this procedure is shown in Figure 9. One should always be careful in applying this kind of image processing techniques because it may introduce an unwanted degree of subjectivity in the resulting patterns. On the other hand, these methods may help to extract some order out of an apparent chaos. Unfortunately, in the resulting model (Figure 9) this goal is only partly reached. Some of the heterogeneities could be related to familiar geological structures such as the Tornquist-Tesseyre zone and the northern edge of the African continent, while other heterogeneities appear to be distributed at random.

In order to establish the significance of these results, the same inversion is performed with synthetic data for a model consisting of nine positive and eight negative point scatterers. The envelope of the resulting model is shown in Figure 10. The heterogeneity is reconstructed near most point scatterers but also in areas away from these point scatterers (Spain, southwest France, Aegean Sea, etc.). This means that even if the data were noise free, there are insufficient data to constrain the resulting model. For noise-corrupted data this effect is aggravated.

Nevertheless, a reasonable good fit of the surface wave coda is achieved, with a variance reduction of 25%. It may appear surprising that the variance reduction is only 25%, despite the fact that the system of linear equations is underdetermined. However, the linear equations are not only underdetermined but also self-contradictory. This can be seen for example in Figures 4*a* and 4*b*, where the average amplitude spectra for the coda show a jagged appearance. (This is even more pronounced for the individual

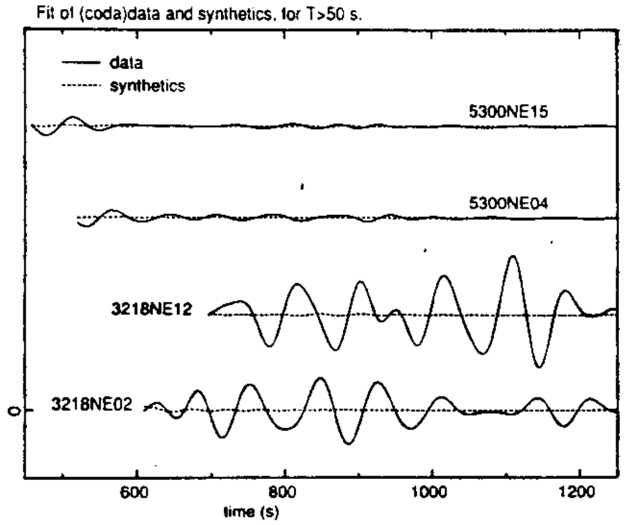

Fig. 11*a*. Examples of the waveform fit of the surface wave coda, low passed at a corner period of 50 s.

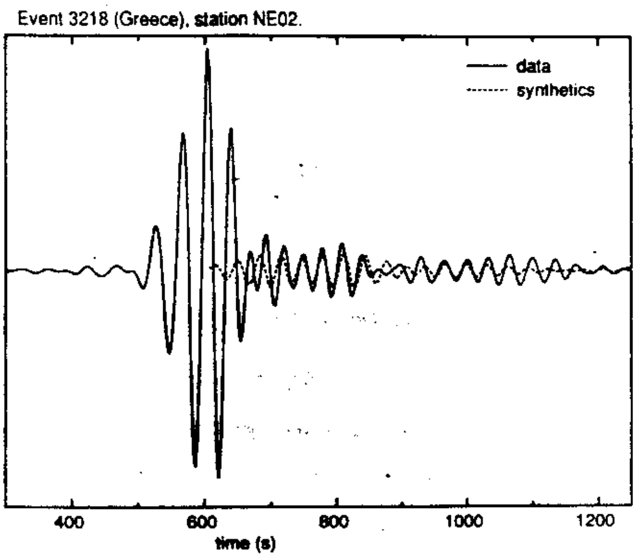

Fig. 12. Full waveform fit of the surface wave coda, high passed at a corner period of 50 s.

spectra.) The scattering theory leads, in general, to much smoother spectra, so that it is impossible to fit all spectral components perfectly, thus producing an imperfect variance reduction.

Some waveform fits of the surface wave coda are shown in Figures 11*a* and 11*b* both low passed and high passed at a corner period of 50 s. For periods larger than 50 s (Figure 11*a*) the waveform fit is poor. This is consistent with the results of section 2, where it was argued that the coda level does not stand out very well above the noise level. However, for the higher frequencies (periods from 30 to 50 s, see Figure 11*b*) a reasonable waveform fit is obtained. Most of the beats in the surface wave coda are reproduced in the synthetics. It should be remembered that the seismograms in these figures only show the surface wave coda. In order to see these data in their proper perspective, a fit of the coda (band passed for periods between 30 s and 50 s) is shown in Figure 12 together with the direct wave. Unfortunately, the fact that good waveform fits are achieved does not establish the reliability of the resulting models because the linear system of equations is underdetermined.

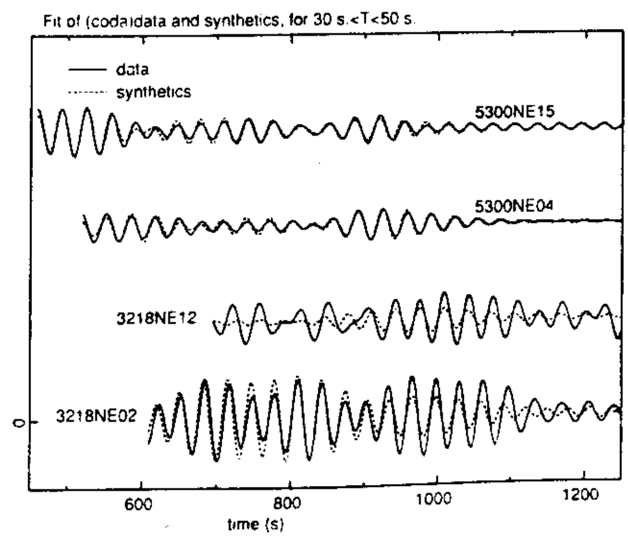

Fig. 11*b*. Examples of the waveform fit of the surface wave coda, high passed at a corner period of 50 s.

Inversions for heterogeneities which extend to a depth different from 170 km produce almost the same model; only the strengths of these heterogeneities differs from the model shown in Figure 8. An inversion for data band passed between 30 and 40 s gives virtually the same result as Figure 8, which confirms that for longer periods the surface wave coda contains a large noise component and not much scattered surface waves.

These results do not imply that mapping lateral heterogeneity using the surface wave coda is impossible. In fact, it has been shown in a controlled field experiment that successful imaging of the surface wave coda is possible [*Snieder*, 1987*a*]. However, the surface wave coda data at our disposal are currently too sparse to produce an accurate reconstruction of the lateral heterogeneity. This is exacerbated by the fact that the noise level in the surface wave coda is relatively high, which can only be compensated with a redundant data set. Large networks of digital seismic stations, as formulated in the ORFEUS [*Nolet et al.*, 1985] and PASSCAL proposals, are necessary to achieve this goal. Alternatively, the Born inversion of the surface wave coda might be used in regional studies where one wishes to study tectonic features such as continental margins or the boundaries of major geological formations. A system of portable digital seismographs would be very useful for this kind of investigations.

The directivity of the solution in Figure 8 is related to the source-receiver geometry. This means that apart from a denser network of stations, we should aim to employ these station in such a way that the wave paths of the recorded waves cover the domain of interest in a more or less homogeneous fashion. Furthermore, three-component data might help to constrain the location of the inhomogeneity because the horizontal components implicitly contain information on the backazimuth from the receiver to the scatterer. Numerical experiments, similar to the experiment that produced Figure 10, could be used to determine which station configuration should be used to image a particular structure. In this way, the design of networks can be related to a particular geophysical or geological problem.

6. BORN INVERSION OF THE DIRECT SURFACE WWAVE

Linear scattering theory can also be used to describe the distortion of the direct wave [*Snieder*, 1987*b*]. This distortion can

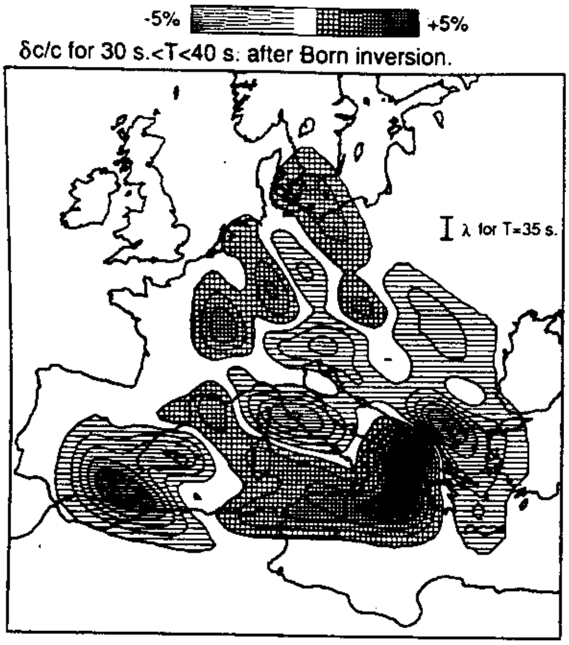

Fig. 13*a*. Relative phase velocity perturbation ($\delta c/c$) for periods between 30 and 40 s as determined from nonlinear waveform inversion plus a subsequent Born inversion. The dominant wavelength of the employed waves is shown for comparison.

either be due to ray geometrical effects or to multipathing effects that are not accounted for by ray theory. In the Born inversion presented in this section, the isotropic approximation is used (paper 1). This means that the relative phase velocity perturbations are retrieved from the linear waveform inversion of the direct wave. This quantity is assumed to be constant within the frequency bands employed (30–40 s, 40–60 s and 60–100 s). (Note that in contrast to the case for the surface wave coda, the direct wave stands out well above the noise level for all employed frequencies; see Figures 4*a* and 4*b*.) A separate Born inversion is performed for each of these frequency bands, so that the phase velocity perturbation is determined independently for each frequency band. In order to justify the isotropic approximation (paper 1), a time window is used to extract the direct wave from the complete seismograms.

The Born inversions presented here are performed for a model of 100×100 cells with a cell size of 35×35 km^2. In the Born inversion of the surface wave coda in section 5, no a priori smoothness constraint was imposed because scattered surface waves are most efficiently generated by sharp lateral heterogeneities. This led to an underdetermined system of linear equations. For the Born inversion of the direct wave the available data set also produces an underdetermined system of linear equations. One alternative would be to increase the cell size, but according to the example of Figure 7 in paper 1, rather small cells are needed to produce the required focusing/defocusing. Instead of this, the smoothing operator of equation (26) in paper 1 is used in this inversion to constrain the solution. In these inversions the values α=0.66 and N=4 are used, which implies an effective correlation length of 140 km. The Born inversions are performed in three iterations (see also paper 1); it has been checked that more iterations do not change the resulting models very much.

The phase velocity perturbation for the three frequency bands are shown in Figure 13. The phase velocities are the result of both the nonlinear inversion for the smooth reference medium and the subsequent Born inversion. See Figure 7*b* as an example of the contribution of the nonlinear inversion for the smooth reference medium to the phase velocity model of Figure 13*c*.

Note that the resulting phase velocity patterns vary considerably on a scale of one horizontal wavelength. This means that ray theory cannot be used to model the effects of these heterogeneities, while surface wave scattering theory takes effects such as multipathing into account. Surprisingly, Figure 13*c* for the phase velocity determined from Born inversion is not too different from Figure 7*a* for the unconstrained nonlinear inversion using

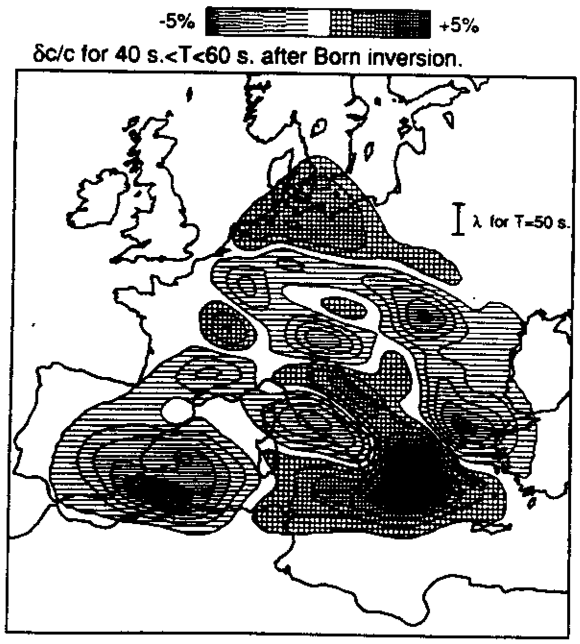

Fig. 13*b*. As Figure 13*a*, but for periods between 40 and 60 s.

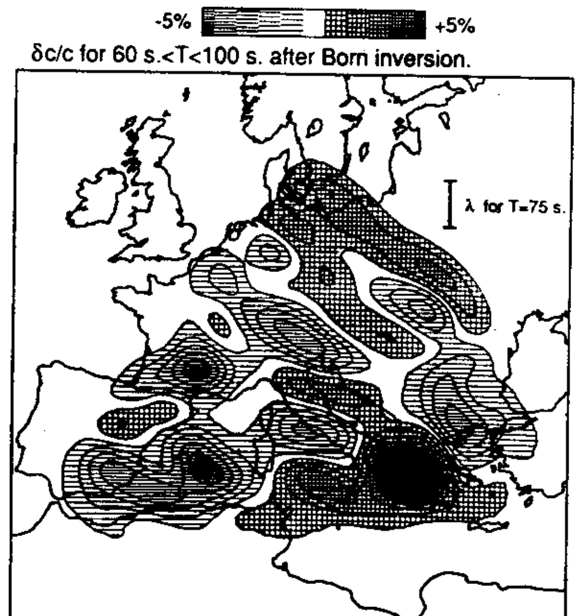

Fig. 13*c*. As Figure 13*a*, but for periods between 60 and 100 s.

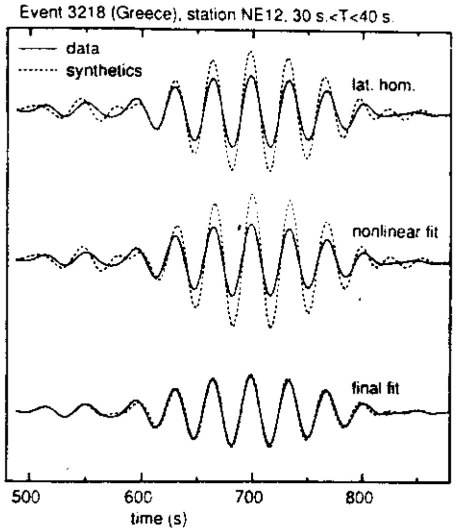

Fig. 14. Waveform fit for periods between 30 and 40 s for the laterally homogeneous starting model (top), after the nonlinear inversion for a smooth reference model (middle), and after Born inversion (bottom), for a Greek event recorded in NE12 (Spain).

ray theory. The smaller-scale features of Figure 13*c* are absent in Figure 7*a* because the spline interpolation does not allow these small-scale features (nor does ray theory). Nevertheless, the overall pattern in these Figures is the same. Apparently, ray theory is rather robust to violations of the requirement that the heterogeneity is smooth. This may explain the success of dispersion measurements in situations where ray theory is not justified. Most of the information on the *S* velocity structure under Europe in the crust and upper mantle is determined from surface wave dispersion measurements. For example, *Panza et al.* [1982] delineated a heterogeneity between Corsica and northern Italy with a scale of approximately 250 km, from anomalously low Rayleigh wave phase velocities between 40 and 60 s. Their results are therefore inconsistent with the (ray) theory that they employed. Nevertheless, this low phase velocity anomaly is also visible in Figure 13*b*, which is constructed using surface wave scattering theory.

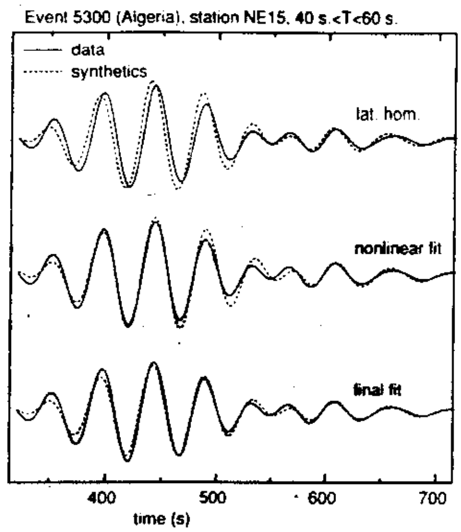

Fig. 16. As Figure 14 for an Algerian event recorded in NE15 (Netherlands) for periods between 40 and 60 s.

Waveform fits after the nonlinear inversion for the smooth reference model and after the subsequent Born inversion (the "final fit") are shown in Figures 14–19. In Figure 14, results for station NE12 near Madrid are shown. The amplitude of the direct surface wave is changed considerably in the inversion. Note that the waveform fit has slightly deteriorated in the nonlinear inversion. The reason for this is that the 42 seismograms are inverted simultaneously, so that it is possible that the fit of one seismogram is improved at the expense of another seismogram. In Figure 15 an example is shown for a seismogram recorded at NE01 (Gothenborg). For this seismogram the amplitude is already quite good for the laterally homogeneous starting model, but the phase is adjusted in the Born inversion. In the preceding examples the Born inversion realized the fit between data and synthetics. This is not the case for all seismograms. In Figure 16 a seismogram for an event in Algeria recorded at NE15 (Netherlands) is shown. For this seismogram the nonlinear inversion performed most of the waveform fit.

By superposing the seismograms for the three frequency bands, seismograms for the full bandwidth (30–100 s) can be

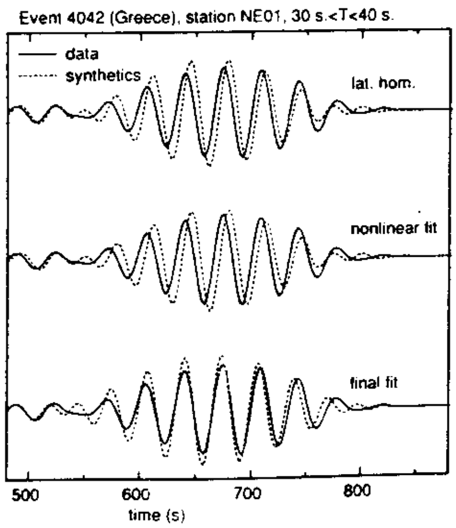

Fig. 15. As Figure 14, for a Greek event recorded in NE01 (Gothenborg) for periods between 30 and 40 s.

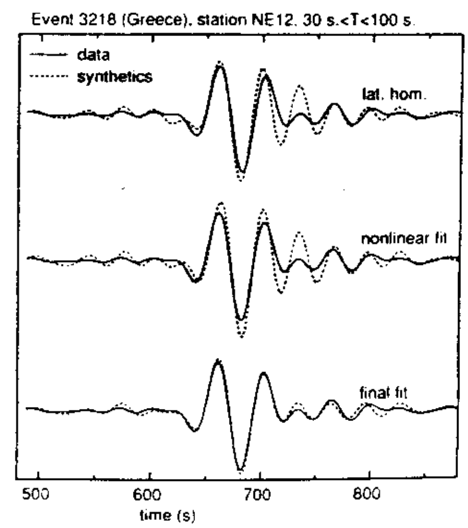

Fig. 17. As Figure 14 for the full bandwidth (30–100 s).

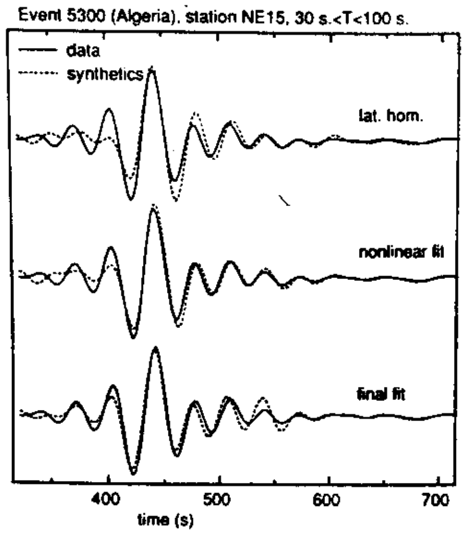

Fig. 18. As Figure 14 for the full bandwidth (30–100 s).

constructed. Figure 17 displays the seismogram of Figure 14, but now for the full employed bandwidth. The final fit between the data and the synthetic is extremely good. Note that the tail of the direct wave (around 725 s) is fitted quite well after the Born inversion. For the recording of the Algerian event in NE15, the full bandwidth data are shown in Figure 18. The trough in the waveform around 420 s has been adjusted well in the nonlinear inversion, whereas the fit of the start of the signal (around 400 s) is improved considerably in the subsequent Born inversion. Unfortunately, the improvement in the waveform fits is not for all seismograms as dramatic as in the preceding examples. Figure 19 features the waveform fit for a Greek event recorded at NE02 (Denmark). The phase of the signal is slightly improved in the nonlinear inversion, but the final waveform fit is not impressive.

The quality of the waveform fits is expressed by the variance reductions shown in Table 1. Both in the nonlinear inversion and in the subsequent Born inversion the variance reduction is of the order of 25%, although this differs considerably between the different frequency bands. In the nonlinear inversion for the smooth reference medium the solution is rather heavily constrained (compare Figures 7*a* and 7*b*) so that larger variance reductions could be achieved with the nonlinear inversion. The smallest variance reduction occurs in the period range from 30 to 40 s. This is not surprising because these surface waves have the shallowest penetration depths and are therefore most strongly subjected to lateral heterogeneity and therefore most difficult to fit. Surprisingly, the variance reduction for periods between 40to 60 s is larger than for 60–100 s. The reason for this might be that surface waves between 60-100 s. are influenced by the low-velocity zone, which is reported to exhibit strong lateral variations [*York and Helmberger*, 1973; *Paulssen*, 1987]. The total variance reduction is larger than the variance reduction obtained by *Yomogida and Aki* [1987] for surface waves which propagated through the Pacific. (They obtained a variance reduction of approximately 30%.) However, it is difficult to compare these results because on the one hand the paths of propagation of the surface waves that they used are much longer than in this study but on the other hand Europe and the Mediterranean is much more heterogeneous than the Pacific.

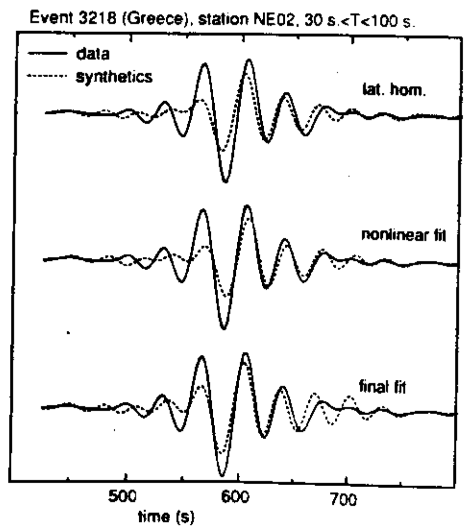

Fig. 19. As Figure 14 for a Greek event recorded in NE02 (Denmark) for the full bandwidth (30–100 s).

TABLE 1. Variance Reductions for the Waveform Inversions

Period, s	Nonlinear	Born	Nonlinear + Born
30-40	15%	20%	31%
40-60	37%	27%	54%
60-100	21%	25%	41%

7. A Resolution Analysis of the Inversion for the Direct Wave

Just as with the inversion for the surface wave coda, the quality of the waveform fit is no measure of the resolution of the inversion. In order to address this issue, synthetics have been

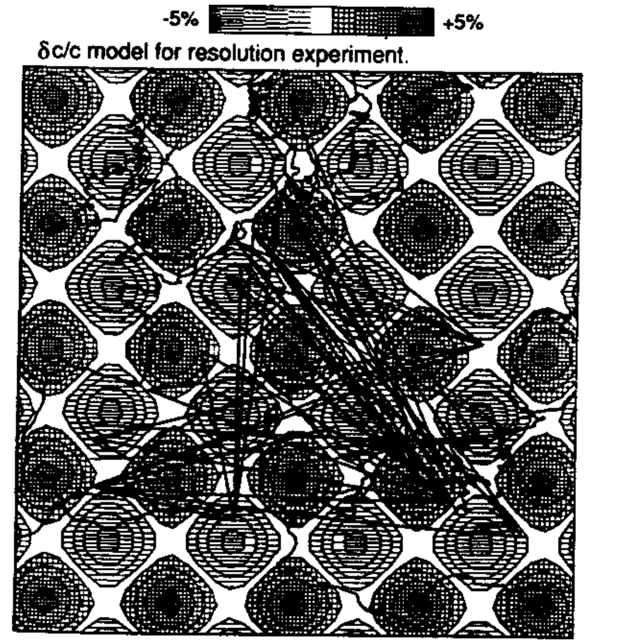

Fig. 20. Synthetic model of the relative phase velocity perturbation ($\delta c/c$) for the resolution experiment of section 7. The source-receiver minor arcs are superposed.

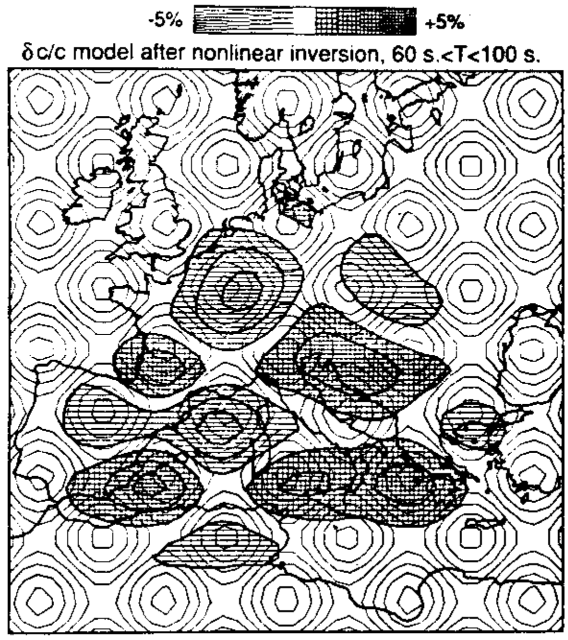

Fig. 21. Reconstruction of the model of Figure 20 after the constrained nonlinear inversion for periods between 60 and 100 s.

computed using asymptotic ray theory [*Woodhouse and Wong*, 1986] for the phase velocity model shown in Figure 20. For convenience, the minor arcs of the used source-receiver pairs are also shown in this Figure. The resulting synthetics have been subjected to the same two-step inversion as the surface wave data from section 6. As a representative example, the results for the period band between 60 and 100 s are presented in this section. In Figure 21 the model as derived in the nonlinear inversion for the smooth reference model is shown. The thin lines show the model of Figure 20; in the ideal case the inversion would reproduce this model. Since only the direct wave is used in this inversion, the solution is only nonzero in the vicinity of the source-receiver minor arcs. Apart from the positive anomaly in the northern Adriatic, the heterogeneities are placed more or less at their correct location. The reconstructed model after the subsequent Born inversion is depicted in Figure 22.

The strength of the model after Born inversion is closer to the true model than after the nonlinear inversion alone. However, the magnitude of the reconstructed heterogeneity is still much less than the magnitude of the input model. The physical reason for this is that the model used in this resolution test consists of alternating positive and negative anomalies. A smearing of these anomalies leads to a reduction of the magnitude of these anomalies. In the true Earth an alternation between positive and negative phase velocity anomalies may also occur, so that the reconstructed models (Figure 13) may underestimate the true phase velocity perturbations.

Surprisingly, the heterogeneities are better positioned after the Born inversion (Figure 22) than after the nonlinear inversion alone (Figure 21). The reason for this is that with the ray geometrical nonlinear inversion one basically measures certain path integrals over the source receiver minor arc (see equations (10a)–(10d) of paper 1), whereas in the Born inversion more complete wave information is used.

It follows from Figure 22 that the east-west resolution in the southern Mediterranean is rather poor. This is due to the fact that there are no crossing rays in that region. A large portion of the wave paths runs in a bundle from Greece to northwestern Europe and encounters a suite of positive and negative anomalies. This leads to a smearing of the solution under Germany and Denmark in the northwest-southeast direction and a subsequent underestimate of the true inhomogeneity. A similar smearing in the northwest-southeast direction is visible in the northern Adriatic; this area also suffers from a lack of crossing ray paths. One of the most conspicuous features in Figure 13 is the high phase velocities under Greece. This is no artifact of the inversion because this feature is not present in the results from the resolution analysis (Figure 22).

In conclusion, the reconstructed phase velocity models are meaningless outside the dotted line in Figures 24 and 25. In the area enclosed by this line, lateral smearing in the northwest-southeast direction occurs under Denmark, Germany, and the northern Adriatic, while there is an east-west smearing in the southern Mediterranean.

8. A MODEL FOR THE S VELOCITY UNDER EUROPE AND THE MEDITERRANEAN

The phase velocity perturbations presented in section 6 can be converted to a depth model using the phase velocity information of the different frequency bands. However, these phase velocities are influenced not only by the composition of the crust and upper mantle but also by the crustal thickness. The crustal thickness under Europe and the Mediterranean is known from refraction studies, and it is therefore possible to correct for the varying crustal thickness. The reference model shown in Figure 6 has a crustal thickness of 33 km. By determining the phase velocity for the same model, but with a different crustal thickness, the following linear parameterization of the effect of crustal thickness on the fundamental Rayleigh mode phase velocity has been determined:

$$\frac{\delta c}{c} = \Gamma\,(z - 33\text{ km})\,(\%) \tag{1}$$

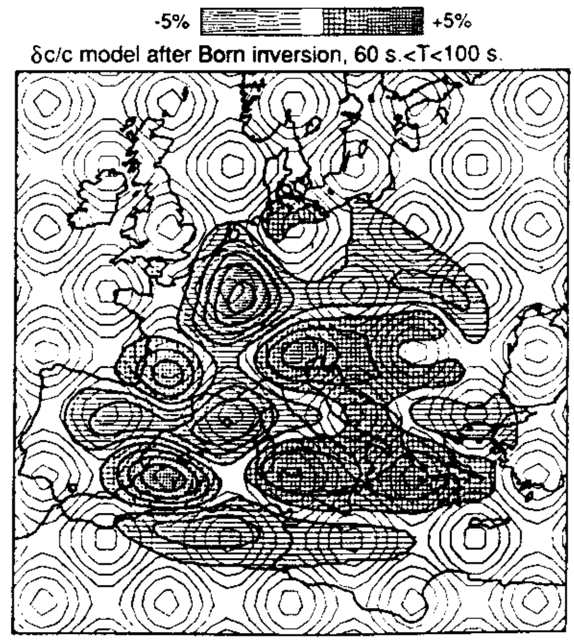

Fig. 22. Reconstruction of the model of Figure 20 after the constrained nonlinear inversion and the subsequent Born inversion for periods between 60 and 100 s.

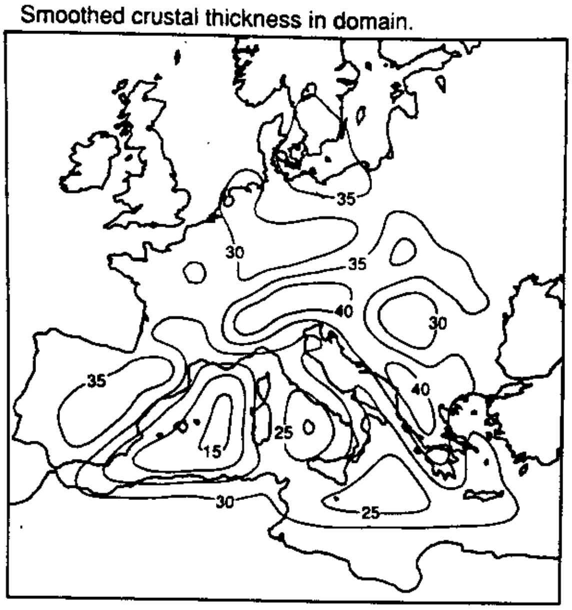

Fig. 23. Smoothed crustal thickness used in the correction for the varying Moho depth.

in this expression, z is the crustal thickness in kilometers.

The parameter Γ is for the different frequency bands given by

$$\begin{aligned} \Gamma &= -0.180\ (\%/\mathrm{km}) \quad \text{for} \quad 30\,s < T < 40\,s \\ \Gamma &= -0.113\ (\%/\mathrm{km}) \quad \text{for} \quad 40\,s < T < 60\,s \qquad (2) \\ \Gamma &= -0.076\ (\%/\mathrm{km}) \quad \text{for} \quad 60\,s < T < 100\,s \end{aligned}$$

The crustal thickness used in this study is adopted from *Meissner* [1986] and *Stoko et al.* [1987], and is shown in Figure 23. In the area outside the dotted line in Figures 24 and 25 the default value is assumed (33 km). For consistency reasons, the same smoothing is applied to the crustal thickness, as for the reconstructions shown in Figure 13. The variations in the crustal thickness are as large as 25 km in the area of interest. For the shortest-period band this leads to a phase velocity perturbation of 4.5%, which is of the same order of magnitude as the perturbations as determined from the Born inversion (Figure 13*a*).

After correcting for the crustal thickness, a standard linear inversion [*Nolet*, 1981] leads to the *S* velocity perturbations for depths between 0 and 100 km, and between 100 and 200 km. A simple resolution analysis shows that incorporating a third layer is unjustified. The resulting *S* velocity perturbations are shown in Figures 24 and 25. A bias in the *S* velocity of the reference model would show up as a dominance of either positive or negative velocity perturbations. Likewise, a bias in the attenuation would show up in structures that would for the majority of the paths produce a marked focusing or defocusing. As can be seen from Figures 24 and 25, and from the wave paths in Figure 1, neither effect seems to be present.

The *S* velocity models in these Figures can be compared with maps of the *S* velocity as compiled subjectively from a wide range of surface wave and body wave data [*Panza et al.*, 1980; *Calcagnile and Scarpa*, 1985]. In general, there is a correspondence of the large-scale features. The velocity is high in the Scandinavian shield, which can be seen in the northern area of inversion of Figures 24 and 25. Under the western Mediterranean the velocity is low [*Marillier and Mueller*, 1985], whereas the Adriatic is characterized by a *S* velocity higher than in the adjacent regions. This high velocity under the Adriatic is more pronounced in the lowest layer (Figure 25) than in the top layer (Figure 24). Note that the Alps do not show up in Figures 24 and 25, whereas *Panza et al.* [1980] and *Calcagnile and Scarpa* [1985] report large anomalies both in the western Alps and the eastern Alps. A reason for this discrepancy might be that the depth-averaged structure of the Alps deviates not very much from the rest of Europe, so that the surface waves are not perturbed strongly.

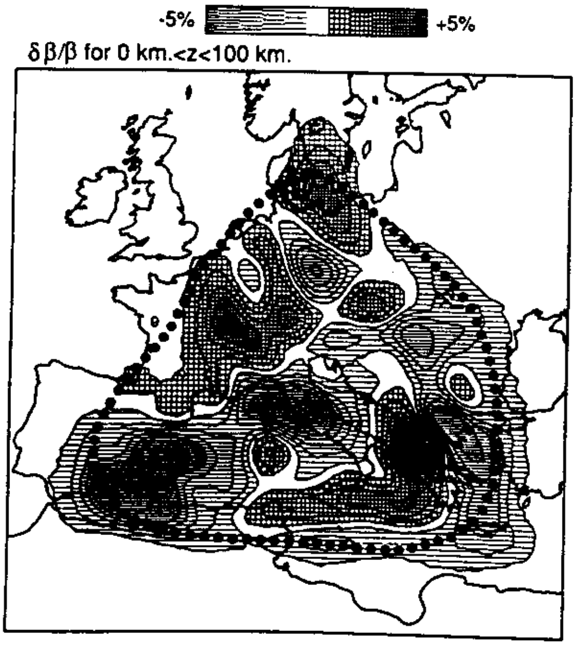

Fig. 24. Relative *S* velocity perturbation ($\delta\beta/\beta$) between the surface and a depth of 100 km.

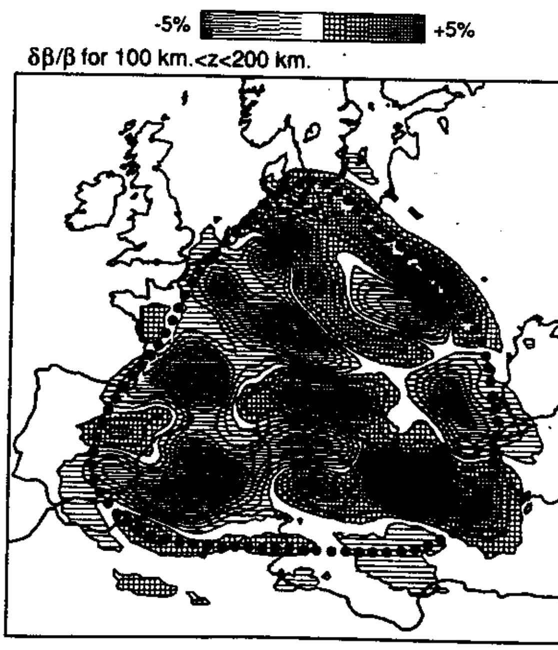

Fig. 25. Relative *S* velocity perturbation ($\delta\beta/\beta$) for depths between 100 and 200 km.

Early tomographic studies using P wave delay times [*Romanowicz*, 1980; *Hovland et al.*, 1981; *Hovland and Husebey*, 1982; *Babuska et al.*, 1984] produced rather different results for the P velocity under Europe. The only consistent features of these studies are the low velocity in the Pannonian basin and the high velocity under the Bohemian massif for the upper layer (0–100 km). Both features can also be seen in Figure 24. (In Figure 23 the Pannonian basin shows up as a region with a thin crust, whereas the Bohemian massif can be identified by its thick crust.) A more recent tomographic inversion with a much larger data set produced more detailed results [*Spakman*, 1986*a,b*; *Spakman et al.*, 1988]. In his studies the subduction of Africa under Europe has been imaged spectacularly. The subduction of Africa of the African slab under Europe can also be seen in Figure 25 as a positive velocity anomaly in the deepest layer (100–200 km) under the Adriatic and northern Italy. *Panza et al.* [1982] observed relatively low velocities in the lid between Corsica and Italy; the same anomaly is visible in Figure 24.

In Figures 24 and 25 the Rhine Graben shows up as a zone of relatively low velocities extending toward the southeast from the Netherlands. Most wave paths in this region are in the southeast-northwest direction. This may explain why in the top layer (Figure 24) only the northern part of the Rhine Graben can be seen, whereas the southern part of the Rhine Graben (which trends in the north-south direction) is not delineated. The variations in the S velocity for the deepest layer (Figure 25) reflect the lateral variations of the low-velocity zone. It is noted by *York and Helmberger* [1973] and *Paulssen* [1987] that strong velocity variations of the low-velocity zone exist, which is confirmed by Figure 25. Under the Massif Central the positive anomaly in the top layer (Figure 24) and the negative anomaly in the bottom layer (Figure 25) indicate a pronounced low-velocity zone, which is consistent with the results of *Souriau* [1981].

The feature which shows the power of the inversion method of this paper most spectacularly is the high-velocity anomaly in eastern Europe in the deepest layer (Figure 25). (It is possible that this area of high velocities extends farther eastward, but this area is not sampled by the data.) From the waveform point of view, this anomaly is needed to produce the focusing needed to fit the amplitudes of seismograms recorded in the northern station of the NARS array. For this reason, this anomaly is located away from (but close to) the source receiver minor arcs. This zone of a high S velocity closely marks the Tornquist-Tesseyre zone, the boundary between central Europe and the east European platform. Note that this transition zone is not visible in the upper layer of the S-velocity model (Figure 24). This is consistent with the findings of *Hurtig et al.* [1979], who showed by fitting travel time curves that below 100 km the eastern European platform has higher P velocities than central Europe. According to Figure 25 this transition at depth between Central Europe and the eastern European platform is very sharp.

The models presented produce a wealth of interesting features. However, at this point one should be extremely careful with a physical interpretation of these models. As shown by the resolution analysis of section 7, parts of these models are subjected to strong lateral smearing, which could produce unwanted artifacts. Furthermore, the number of seismograms that contributes to the reconstruction of a particular inhomogeneity is relatively small. This means that errors in individual seismograms can distort the reconstructed images. Larger data sets with a more even path distribution are needed to produce models which are less likely to contain artifacts and which are more robust to errors in individual seismograms.

9. CONCLUSION

Linear inversion of a large set of surface wave data is feasible with present-day computers. The Born inversion for the surface wave coda (using 42 seismograms) ran in roughly one night on a super minicomputer. The inversion of the direct surface wave for the three frequency bands takes approximately the same time. The nonlinear inversion for the smooth reference model is comparatively fast and takes about 3 hours for the three frequency bands. With the present growth in computer power, larger data sets can soon be inverted with the same method, possibly on a global scale.

Reasonable waveform fits of the surface wave coda can be obtained, leading to a variance reduction of approximately 25% for the surface wave coda. However, with the data set used in this study many artifacts are introduced in the inversion (the analogue of the smiles in exploration seismics). The fact that the surface wave coda contains a relatively large noise component is an extra complication. A larger (redundant) data set is needed to perform an accurate imaging of the inhomogeneity in the Earth using the surface wave coda. It would be interesting to set up controlled experiments to probe tectonic structures like continental margins or the Tornquist-Tesseyre zone with scattered surface waves.

Application of Born inversion to the direct surface waves leads to detailed S velocity models on a scale comparable to the wavelength of the surface waves used. With the data set employed, a lateral resolution of approximately 300 km can be achieved in some regions (Italy, France, Alps, western Mediterranean), while in other areas, smearing along the wave paths occurs (southern Mediterranean, northeastern Europe, the Adriatic). More data are needed to achieve a more evenly distributed resolution. Only a limited depth resolution can be obtained.

The fact that a model of the heterogeneity is constructed with a horizontal length scale comparable to the wavelength of the used surface waves implies that scattering and multipathing effects are operative. This means that for this situation, dispersion measurements are not justified. Nevertheless, the resulting model for the S velocity bears close resemblance to the S velocity models constructed by *Panza et al.* [1980] and *Calcagnile and Scarpa* [1985], which are largely based on surface wave dispersion measurements. Apparently, the phase as deduced from ray theory is relatively robust for structures that are not smooth on scale of a wavelength.

Linear waveform inversion is a powerful and rigorous method to fit surface wave data. Presently, the main limitation is imposed by the availability of high-quality digital surface wave data. A network of seismometers, as described in the ORFEUS [*Nolet et al.*, 1985] or PASSCAL proposals, will increase the resolution and reliability of the resulting models. A data distribution center like ODC (ORFEUS Data Center) provides access to digital seismological data at low costs. Born inversion for surface waves, applied to these data, may help to construct accurate S velocity models of the Earth.

Acknowledgments. I thank Guust Nolet for his stimulating interest and advice for this research. His nonlinear waveform fitting program formed the backbone of the nonlinear waveform inversion presented in this study. Wim Spakman provided me kindly with his tomography program, which formed the basis for the software for the Born inversion. The help of Gordon Shudofsky, Bernard Dost, and Hanneke Paulssen was indispensable for handling the NARS data. The constructive comments of Brian Mitchell and an anonymous reviewer are greatly appreciated. The NARS project has been funded by AWON, the Earth Science branch of the Netherlands Organization for the Advancement of Pure Research (ZWO).

JOURNAL OF GEOPHYSICAL RESEARCH, VOL. 93, NO. B10, PAGES 12,055–12,065, OCTOBER 10, 1988

Large-Scale Waveform Inversions of Surface Waves for Lateral Heterogeneity
1. Theory and Numerical Examples

ROEL SNIEDER

Department of Theoretical Geophysics, University of Utrecht, The Netherlands

Surface wave scattering theory is presented as a new method for analyzing teleseismic surface wave data. Using surface wave scattering integrals the effect of lateral heterogeneity both on the surface wave coda generation and on the direct surface wave is described. Since the employed scattering theory for the forward problem is linear, the inverse problem can conveniently be solved in the least squares sense using an iterative matrix solver. For waveform inversions of the direct surface wave, only near forward scattering contributes. For this case the isotropic approximation is introduced, which makes it possible to retrieve phase velocity information from scattering theory. It is shown that for practical waveform inversions the resulting system of linear equations is extremely large and how row action methods can be used conveniently for carrying out the inversion on moderate size computers. The performance of the inversions is illustrated with two numerical examples. In the first example the surface wave coda generated by one point scatterer is inverted. It is shown that the reconstruction in this case is similar to Kirchhoff migration methods as used in exploration seismics. In the second example, ray geometrical effects (focusing and phase shifting) are obtained from the linear inversion with scattering theory. It follows from this example that linear waveform inversion can simultaneously fit the amplitude and the phase of surface wave data.

1. Introduction

Standard surface wave analysis proceeds by extracting path-averaged group or phase velocities from surface wave data using dispersion analysis. If sufficient data are available, these path-averaged dispersion data can be used to determine the local phase or group velocity. Mathematically, this approach relies on the great circle theorem [*Backus*, 1964; *Jordan*, 1978; *Dahlen*, 1979] or more accurately on the minor arc theorem [*Romanowicz*, 1987]. These theorems state that surface waves are only influenced by the integral of the phase or group velocity over the source receiver great circle (or minor arc). This is justified if the lateral heterogeneity is smooth on a scale of a wavelength of the surface waves under consideration.

In practice, this condition may not be satisfied. For example, a 30-s Rayleigh wave has a wavelength of approximately 120 km. In continents the lateral variation on this scale can be considerable, so that the use of the great circle (minor arc) theorem and the related dispersion measurements are not justified. Surprisingly, this well-known fact is widely ignored, and in some cases, dispersion analysis is used over structures which have the same length scale as the surface waves [e.g., *Panza et al.*, 1980; *Calcagnile and Scarpa*, 1985]. If the structure is not smooth on a scale of a wavelength, surface wave scattering and multipathing may occur. This is documented for reflection of surface waves at a continental margin by *Levshin and Berteussen* [1979] and *Bungum and Capon* [1974]. Linearized scattering theory can be used to describe these effects. This theory is developed both for a flat geometry [*Snieder*, 1986*a*,*b*], and for a spherical geometry [*Snieder and Nolet*, 1987].

Scattered surface waves must to some degree be responsible for the generation of the surface wave coda, and it would be fruitful to extract this information from the surface wave coda. *Snieder* [1986a] presents a holographic inversion scheme for the surface wave coda, reminiscent of migration procedures in exploration seismics. This inversion method has been applied successfully to image the surface wave reflections from a concrete dam on a tidal flat [*Snieder*, 1987*a*]. In order to achieve this, several severe approximations have been used, and it is desirable to give waveform inversion for surface data a firmer theoretical basis. This paper serves to provide a rigorous waveform-fitting method for surface waves, based on surface wave scattering theory. This inversion is set up as a huge matrix problem, and it is shown how solutions can be found iteratively.

There is, however, more to be gained from surface wave scattering theory than an analysis of the surface wave coda. Surface wave scattering theory can also be used to describe the distortion of the direct wave due to lateral heterogeneity [*Snieder*, 1987*b*]. This allows not only for accurate forward modeling of the direct surface wave in the presence of lateral heterogeneity but also for a waveform inversion of the direct surface wave train. In this way both amplitude and phase information can be used.

A waveform inversion of surface wave data was first attempted by *Lerner-Lam and Jordan* [1983], who linearly fitted higher-mode surface waves with a laterally homogeneous model. *Nolet et al.* [1986*a*] extended this method to incorporate nonlinear effects and lateral inhomogeneity. However, they only used the phase information of the surface waves. *Yomogida and Aki* [1987] used the Rytov field to fit both the amplitude and phase of fundamental mode Rayleigh wave data. The starting point of *Yomogida and Aki* [1987] is the two-dimensional wave equation. One can argue that their method lacks rigor because it is not clear that surface waves satisfy the two-dimensional wave equation. *Tanimoto* [1987] determined a global model for the *S* velocity in terms of spherical harmonics up to order 8 using long-period higher-mode waveforms. In computing the synthetics he used the great circle theorem to compute the phase shift, and he ignored focusing effects. Because of the low order of his spectral expansion ($l \leq 8$), ray theory could be used for this inversion. This means that up to this point, all waveform inversions for surface waves relied either on ray theory or on the two-dimensional wave equation.

In this paper it is shown how linear scattering theory can be used for waveform fitting of the direct surface wave by the reconstruction of a two-dimensional phase velocity field. The derivation uses the full equations of elasticity, and neither uses ray

Paper number 7B6093.
0148-0227/88/007B-6093$05.00

theory nor the two-dimensional wave equation. Specifically, there is no need to assume any smoothness properties of the medium. In fact, in section 7 a numerical example is shown of the distortion of the direct surface wave by a structure with sharp edges. A restriction of this inversion method is that small scattering angles are assumed. This can in practice be realized by time windowing the data.

In section 2 some elements of surface wave scattering theory are revisited. The isotropic approximation, which allows the determination of phase velocities from scattering theory, is introduced in section 3. Section 4 features a method to invert the resulting scattering integral. Due to the extremely large size of the resulting matrix equation this is not without problems, and in section 5, several tricks are shown to make these computations feasible on systems as small as a super minicomputer. Unfortunately, the surface wave inversion problem is in reality nonlinear, and the assumption of linearity is only justified for reference models which are sufficiently close to the real Earth. It is therefore advantageous to perform a nonlinear inversion (using ray theory) first (section 6) in order to find a smooth reference model for the subsequent linear inversion. (In this paper this linear inversion is referred to as "Born inversion.") In section 7 it is shown that a more or less realistic distribution of scatterers produces a realistic looking coda but also that sharp lateral heterogeneity may severely distort the direct surface wave. Examples of inversions for a point scatterer and for ray geometrical effects (phase shifting and focusing) are presented in the last two sections. Application of this technique to surface wave data recorded with the Network of Autonomously Recording Seismographs (NARS) are presented by *Snieder*, [this issue] (hereafter referred to as paper 2).

Throughout this paper the limitations of surface wave scattering are assumed [*Snieder and Nolet*, 1987]; that is, it is assumed that the heterogeneity is weak and that the far-field limit can be used. In order to transcend these limitations a considerable amount of theoretical work remains to be done. For reasons of simplicity, only vertical component fundamental mode data are assumed, but this restriction is not crucial. Note that this does not mean that the fundamental Love wave need not be considered, because in general a double-couple source excites Love waves, which may be converted by the heterogeneity to Rayleigh waves.

2. SURFACE WAVE SCATTERING THEORY

A dyadic decomposition of the surface wave Green's function [*Snieder*, 1986*a*; *Snieder and Nolet*, 1987] has allowed compact expressions for both the direct and the scattered surface waves. In this section, elements of surface wave scattering theory are briefly presented. Throughout this paper a spherical geometry is assumed, and computations are performed to leading order of ka, where k is the wave number and a the circumference of the Earth. As shown by *Snieder and Nolet* [1987], the unperturbed surface wave excited by a moment tensor **M** can be written as a sum over surface wave modes (with index ν):

$$\mathbf{u}^0(r,\theta,\phi) = \sum_\nu \mathbf{p}^\nu(r,\mu_R)\,\frac{e^{i(k_\nu a\Delta+\frac{\pi}{4})}}{\sqrt{\sin\Delta}}\,(\mathbf{E}^{\nu*}(r_S,\mu_S):\mathbf{M}) \qquad (1)$$

In this expression, μ_S and μ_R are the azimuths of the source receiver minor arc at the source and receiver, respectively, counted anticlockwise from south, while Δ is the epicentral distance. In this paper we shall only be concerned with the fundamental modes, so that the (Greek) mode indices are usually omitted. The polarization vector **p** is for Love waves given by

$$\mathbf{p}_L = -(l+\tfrac{1}{2})\,W(r)\,\hat{\boldsymbol{\phi}} \qquad (2a)$$

and for Rayleigh waves by

$$\mathbf{p}_R = (l+\tfrac{1}{2})\,V(r)\,\hat{\boldsymbol{\Delta}} - iU(r)\hat{\mathbf{r}} \qquad (2b)$$

where $\hat{\mathbf{r}}$, $\hat{\boldsymbol{\Delta}}$, and $\hat{\boldsymbol{\phi}}$ are unit vectors in the vertical, radial, and transverse direction, respectively. The eigenfunctions U, V, and W of the Earth's normal modes are defined by *Gilbert and Dziewonski* [1975]. The eigenfunctions are assumed to be normalized as by *Snieder and Nolet* [1987]:

$$\tfrac{1}{2}\int \rho(r)\left[U^2(r)+l(l+1)V^2(r)\right]r^2dr =$$
$$\tfrac{1}{2}\int \rho(r)\,l(l+1)W^2(r)\,r^2dr = \left[\frac{l+\frac{1}{2}}{2\pi}\right]^{\frac{1}{2}} /4\omega u_g \qquad (3)$$

The angular quantum number l is related to the wave number by the relation $ka = l+\frac{1}{2}$, and u_g is the angular group velocity of the mode under consideration. The excitation tensor **E** in (1) can be expressed in the polarization vector at the source

$$\mathbf{E}(r_S,\mu_S) = \left\{\hat{\mathbf{r}}\partial_r + i\frac{(l+\frac{1}{2})}{r}\hat{\boldsymbol{\Delta}}_S\right\}\mathbf{p}(r_S,\mu_S) \qquad (4)$$

The perturbation of the wave field due to the lateral heterogeneity can be expressed as a double sum over incoming (σ) and scattered (ν) surface waves modes [*Snieder and Nolet*, 1987]

$$\mathbf{u}^1(r,\theta,\phi) = \sum_{\nu,\sigma}\iint \mathbf{p}^\nu(r,\mu_R')\,\frac{e^{i(k_\nu a\Delta_2+\frac{\pi}{4})}}{(\sin\Delta_2)^{\frac{1}{2}}}\,V^{\nu\sigma}(\theta',\phi')\times$$
$$\times\frac{e^{i(k_\sigma a\Delta_1+\frac{\pi}{4})}}{(\sin\Delta_1)^{\frac{1}{2}}}\,(\mathbf{E}^{\sigma*}(r_S,\mu_S').\mathbf{M})\,d\Omega' \qquad (5)$$

The surface wave distortion is expressed as a scattering integral over the horizontal extend of the heterogeneity (θ',ϕ'). The minor arc from the source to the heterogeneity (θ',ϕ') defines the azimuth μ_S' at the source and the angular distance Δ_1, while the minor arc from (θ',ϕ') to the receiver defines the azimuth μ_R' at the receiver and the angular distance Δ_2. The interaction matrix $V^{\nu\sigma}$ describes the coupling between the modes ν and σ. For isotropic perturbations in the density $\delta\rho$ and the Lamé parameters $\delta\lambda$ and $\delta\mu$ the interaction matrix depends only on frequency and the scattering angle Ψ defined by

$$\Psi = \mu_{out} - \mu_{in} \qquad (6)$$

(μ_{out} and μ_{in} are the azimuths of the incoming and scattered wave at the scatterer.) Extensions for perturbations of interfaces and gravitational effects are given by *Snieder and Romanowicz* [1988], while the effects of anisotropy are discussed by *Romanowicz and Snieder* [1988].

For perturbations in the density and the Lamé parameters the interaction terms are depth integrals containing the heterogeneity and the modes under consideration [*Snieder and Nolet*, 1987]. For example, the Love wave to Rayleigh wave conversion ($R \leftarrow L$) is given by

$$V_{RL} = (l_R+\tfrac{1}{2})(l_L+\tfrac{1}{2})\int\Big[-V_R W_L\,\delta\rho\omega^2$$
$$+\left(\frac{1}{r}U_R+\partial_r V_R\right)(\partial_r W_L)\delta\mu\Big]\,r^2dr\,\sin\psi$$

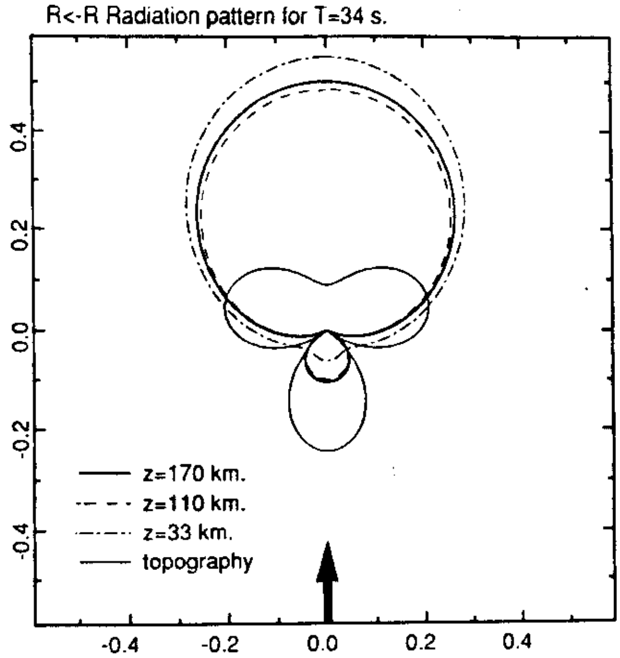

Fig. 1*a*. Radiation pattern for the interaction of the fundamental Rayleigh mode with itself for surface topography (3 km) and for *S* velocity perturbations extending down to 170 km ($\delta\beta/\beta$=4%), 110 km ($\delta\beta/\beta$=4%), and 33 km ($\delta\beta/\beta$=12%). The effective size of the scatterer is 100×100 km^2. The direction of the incoming wave is shown by an arrow.

$$+ (l_R+½)^2(l_L+½)^2 \int V_R W_L \delta\mu \, dr \, \sin 2\psi \qquad (7)$$

For Love-Love wave interactions (*LL*) or Rayleigh-Rayleigh wave interactions (*RR*) a similar dependence on the scattering angle exists

$$\tilde{V}_{RR \text{ or } LL} = \tilde{V}_{RR}^{(0)} + \tilde{V}_{RR \text{ or } LL}^{(1)} \cos \Psi + \tilde{V}_{RR \text{ or } LL}^{(2)} \cos 2\Psi \qquad (8)$$

In Figures 1*a* and 1*b* the radiation patterns are shown for interactions of the fundamental Rayleigh wave with itself and for conversion from the fundamental Love wave to the fundamental Rayleigh wave. These radiation patterns are shown for surface topography [*Snieder*, 1986*b*; *Snieder and Romanowicz*, 1988], and for a constant relative perturbation in the *S* velocity $\delta\beta/\beta$ down to different depths with an unperturbed density ($\delta\rho$=0). The perturbations in the Lamé parameters are equal.

It is shown by *Snieder* [1986*b*] that the interaction terms for forward scattering and unconverted waves are proportional to the perturbation of the phase velocity δc. Using the normalization (3), equation (9.3) of *Snieder* [1986*b*] can be written as

$$\frac{\delta c}{c} = \left[\frac{2\pi}{l+½}\right]^{½} \frac{1}{(l+½)} \tilde{V}^{unconverted}(\Psi{=}0) \ . \qquad (9)$$

Up to this point, it has been assumed that the real Earth can be treated as a radially symmetric reference model (producing a seismogram $\mathbf{u}^0$), with superposed lateral inhomogeneities (leading to the seismogram distortion $\mathbf{u}^1$). However, as shown in *Snieder* [1986*a*], the theory can also be formulated for a smoothly varying reference model, with embedded heterogeneities. (Smooth means that the lateral variation is small on a scale of one horizontal wavelength.) In that case the phase terms and the geometrical spreading terms of the propagators follow from ray theory [*Snieder*, 1986*a*]. Solving the ray tracing equations is a cumbersome affair, and as long as the inhomogeneity of the reference medium is sufficiently weak, the ray geometrical effects can be expressed as simple line integrals over the minor arc under consideration [*Woodhouse and Wong*, 1986; *Romanowicz*, 1987]. Using these results, the propagator terms $\exp i(ka\Delta+\pi/4)/\sqrt{\sin\Delta}$ in (1) and (5) should for the case of a smooth reference medium be replaced by

$$ka\Delta \rightarrow ka\left[\Delta - \int_0^{\Delta} \frac{\delta c}{c}\, d\Delta'\right] \qquad (10a)$$

$$\sin\Delta \rightarrow \sin\Delta - \int_0^{\Delta} \sin\Delta' \sin(\Delta-\Delta')\, \partial_{nn}\left(\frac{\delta c}{c}\right) d\Delta' \qquad (10b)$$

The azimuth terms in the polarization vectors and the scattering angle should be replaced by

$$\mu_S \rightarrow \mu_S - \frac{1}{\sin\Delta} \int_0^{\Delta} \sin(\Delta-\Delta')\, \partial_n\left(\frac{\delta c}{c}\right) d\Delta' \qquad (10c)$$

$$\mu_R \rightarrow \mu_R + \frac{1}{\sin\Delta} \int_0^{\Delta} \sin\Delta'\, \partial_n\left(\frac{\delta c}{c}\right) d\Delta' \qquad (10d)$$

with similar expressions for the azimuths of the incoming and outgoing wave at the scatterer. In these expressions, $\delta c/c$ is the relative phase velocity perturbation of the reference medium, while ∂_n and ∂_{nn} are the first and second angular derivatives in the transverse direction.

One should be careful giving $\mathbf{u}^1$ the interpretation of the scattered surface wave because $\mathbf{u}^1$ describes all perturbations of the wave field due to the perturbations superposed on the reference medium. If there are abrupt lateral variations, this leads to surface wave scattering. However, in the case of a smoother perturbation on the reference model, $\mathbf{u}^1$ describes the change in the direct wave due to these inhomogeneities. For example, it is shown explicitly by *Snieder* [1987*b*] that the "scattering integral"

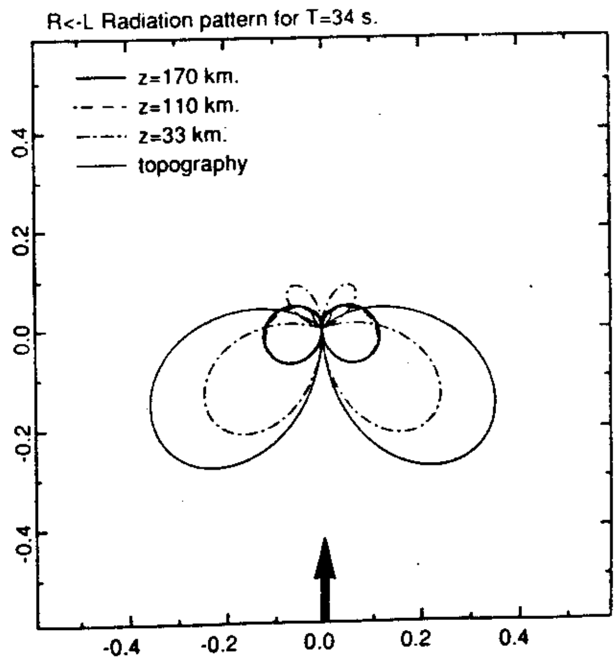

Fig. 1*b*. Radiation pattern for the conversion from the fundamental Love mode to the fundamental Rayleigh mode. Conventions as in Figure 1*a*.

(5) describes the ray geometrical effects on the direct wave due to smooth lateral heterogeneity.

3. Isotropic Approximation

The surface wave scattering formalism, as presented in section 2, establishes a linear relation between the lateral heterogeneity and the perturbations of the surface wave field. In principle, a three-dimensional inversion could therefore be formulated as a huge system of linear equations by discretizing both the scattering integral over the heterogeneity (5) and the depth integrals in the interaction terms (7). Unfortunately, the simplicity of this approach is elusive. An inversion using the surface wave scattering integral (5) should take care of the following effects: (1) The inhomogeneities should be located at their correct horizontal position. (2) The depth distribution of the heterogeneity should be determined. (3) The contributions from the different inhomogeneities $\delta\rho$, $\delta\lambda$, and $\delta\mu$ should be unravelled. It is difficult those achieve these goals, since the heterogeneity acts on the wave field only through the interaction terms $V^{\nu\sigma}$. This means that it is only possible to retrieve certain depth integrals of the heterogeneity. Information for different frequencies, and possibly different modes, is needed for the reconstruction of the depth dependence of the inhomogeneity. The contribution of the different types of inhomogeneity $(\delta\rho, \delta\lambda, \delta\mu)$ can only be retrieved by using information of different scattering angles.

It will be clear that a complete three-dimensional reconstruction of the heterogeneity is hard to realize with a finite set of band-limited, noise-contaminated data. With present data sets there are two realistic approaches. One can parameterize the depth dependence and the different contributions of $\delta\rho$, $\delta\lambda$, and $\delta\mu$ in a finite set of basis functions. This reduces the degrees of freedom of the heterogeneity, which facilitates a well-behaved inversion. This approach has been taken in a field experiment where surface waves on a tidal flat were reflected by a concrete dam [*Snieder*, 1987*a*]. In this test example the depth dependence of the heterogeneity was prescribed, and an accurate reconstruction of the location of the dam was realized using the surface wave coda.

Alternatively, one can make the "isotropic approximation." It follows from (8) that the $R \leftarrow R$ radiation pattern is stationary with respect to the scattering angle for near forward directions. This can be verified in Figure 1*a* for several different inhomogeneities. Furthermore, it follows from (7) that the $R \leftarrow L$ conversion vanishes in the forward direction. From Figure 1*b* it can be seen that for the shown examples the $R \leftarrow L$ conversion is small for near forward directions. This means that (at least for the fundamental modes) for near forward directions one can make the "isotropic approximation." This means that

$$V_{RL} \approx 0 \tag{11}$$

$$V_{RR} \approx V_{RR}^{(0)} + V_{RR}^{(1)} + V_{RR}^{(2)} = -\left(\frac{l+½}{2\pi}\right)^{½} (l+½)\,\frac{\delta c}{c} \tag{12}$$

These expressions are extremely useful because they make it possible to retrieve the phase velocity perturbation from scattering theory. This allows a two-stage inversion of surface wave data. In the first step the scattering theory is used to find the phase velocity perturbation using (5), (11), and (12). Once these local phase velocities are computed, a standard linear inversion can be used to determine the depth dependence of the heterogeneity [*Nolet*, 1981]. The catch is that this approach forces us to use information for small scattering angles only. In practice, this can be achieved by time windowing the seismograms, and only using the information contained in the direct wave. Note that there are no smoothness restrictions on the heterogeneity, so that it is in principle possible to reconstruct a two-dimensional phase velocity field without doing any dispersion measurements. In this way, the conditions for the validity of the great circle theorem need not be fulfilled.

4. Inversion of the Scattering Integral

The linear relation (5) between the perturbation of the wave field and the perturbation of the medium can be written as

$$\mathbf{u}^1 = \sum_{\nu,\sigma} \iint \mathbf{p}^{\nu} g_{\nu}(\Delta_2)\, \frac{\partial V^{\nu\sigma}}{\partial m} \cdot m(\theta',\phi')\, g_{\sigma}(\Delta_1)\, (\mathbf{E}^{\sigma*} : \mathbf{M})\, d\Omega' \tag{13}$$

with the propagators defined by

$$g_{\nu}(\Delta) = \frac{e^{i\left(k_{\nu} a \Delta + \frac{\pi}{4}\right)}}{\sqrt{\sin \Delta}} \tag{14}$$

or its equivalent for a smoothly varying reference medium (10). The model parameter m designates either the heterogeneity $(\delta\rho, \delta\lambda, \delta\mu)$ parameterized in some suitable form or the phase velocity perturbation $\delta c/c$ if the isotropic approximation is used. The difference between the recorded surface wave data and the synthetics for the reference model ($\mathbf{u}^0$) can for all events, stations, and frequency components be arranged in one (huge) vector $\mathbf{d}$ of data residuals. Likewise, the model parameters can, after a discretization in cells of the surface integral (13) (and possibly also of the depth integrals in the interaction terms), be arranged in one model vector $\mathbf{m}$. (Of course, one does not have to expand the heterogeneity in cells; other parameterizations can also be used.) In that case, (13) can be written as a matrix equation

$$d_i = \sum_j G_{ij} m_j \tag{15}$$

where G_{ij} is the spectral component of the synthetic seismogram for event-station pair "i" at frequency ω_i, due to a unit perturbation of model parameter "j."

In general, the matrix $\mathbf{G}$ is extremely large. The reason for this is that the integrand in the original scattering equation (13) is rapidly oscillating with the position of the inhomogeneity. This means that in order to discretize (13) accurately, a cell size much smaller than a wavelength is needed. For an inversion on a continental scale for surface waves with a wavelength of say 100 km, several thousands of cells are needed. Fortunately, extremely large systems of linear equations can be solved iteratively in the least squares sense (Van der Sluis and Van der Vorst, 1987), so that a brute force inversion of $\mathbf{G}$ need not be performed. The least squares solution minimizes the misfit $|\mathbf{d}-\mathbf{Gm}|^2$, so that one performs in fact a least squares waveform fit of the data residual $\mathbf{d}$ to the synthetics $\mathbf{Gm}$.

In the inversions presented in this paper, and in paper 2, the algorithm LSQR of *Paige and Saunders* [1982*a*,*b*] is used to solve (15) iteratively in the least squares sense. LSQR performs the inversion by doing suitable matrix multiplications with $\mathbf{G}$ and $\mathbf{G}^T$. (In the language of modern optimization schemes [*Tarantola and Valette*, 1982], one would say that one only needs to solve the forward problem.) There is no need to store the matrix in memory; in fact, one only needs to supply LSQR with a subroutine to do a multiplication with one row of $\mathbf{G}$ or $\mathbf{G}^T$. As an additional advantage, LSQR has convenient "built in" regularization properties [*Van der Sluis and Van der Vorst*, 1987]. The stability of LSQR is confirmed by *Spakman and Nolet* [1987], who applied LSQR to a tomographic inversion of an extremely large set of P

wave delay times and who made a comparison with other iterative solvers of linear equations.

The inversion with LSQR has some interesting similarities with migration methods in exploration seismics. The first iteration of LSQR yields a solution proportional to $\mathbf{G}^T\mathbf{d}$, higher iterations perform corrections to the misfit [*Van der Sluis and Van der Vorst*, 1987]. It is shown in detail by *Snieder* [1987*a*] that the contraction $\mathbf{G}^T\mathbf{d}$ amounts to a holographic reconstruction of the heterogeneity. This means that the waves propagating away from the sources (the illumination) are correlated with the surface wave residuals which have back propagated from the receivers into the medium. For one source-receiver pair this leads to an ellipsoidal contribution to the reconstructed image. By summing over all source-receiver pairs (which is implicit in the product $\mathbf{G}^T\mathbf{d}$) an image is constructed. It is shown by *Tarantola* [1984*a,b*] that this procedure is similar to Kirchhoff migration as used in exploration seismics. Just as with these techniques, the surface wave reconstructions using the method of this paper will contain "smiles" [*Berkhout*, 1984] if insufficient data are used.

It may be advantageous to impose an a priori smoothness constraint on the solution. This can be achieved by solving instead of (15) the matrix equation

$$\mathbf{G}\mathbf{S}\tilde{\mathbf{m}} = \mathbf{d} \tag{16}$$

where S is a prescribed smoothing matrix. This yields the solution

$$\mathbf{m} = \bar{\mathbf{S}}\tilde{\mathbf{m}} \tag{17}$$

which incorporates the smoothness criterion imposed by S.

5. Practical Implementation of Solving the Matrix Equation

Solving the linear system (15) or (16) is not entirely straightforward because the matrix may be extremely large. For example, discretizing the continent of Europe (with a size of say $3500\times3500\ \mathrm{km}^2$) in cells of $35\times35\ \mathrm{km}^2$ (which is 1/4 of the wavelength of a 30-s fundamental mode Rayleigh wave) leads to a model of 10,000 cells. For the data set used in paper 2, there are approximately 2500 spectral components of surface wave data to be fitted. This means that storing this matrix requires 100 Mbyte of disc space, which is impractical (if not impossible on many machines). As mentioned before, LSQR does not need the whole matrix at once but only needs access to the rows of G and $\mathbf{G}^T$. In principle, the matrix can therefore be computed during the inversion. However, due to the large number of trigonometric operations required for the computation of the synthetics this leads to prohibitive CPU times.

If we restrict ourselves to vertical component data for the fundamental mode only, the elements of the matrix G have the form

$$G = A_R e^{i\phi_R} + A_L e^{i\phi_L} \tag{18}$$

The first term in this expression describes the scattering of the fundamental Rayleigh mode to itself, while the second term describes the conversion from the fundamental Love mode to the fundamental Rayleigh mode. The terms ϕ_R and ϕ_L are the phase terms of the propagators (14), while the complex amplitudes A_R and A_L contain the remaining terms.

Due to the phase terms, the matrix G_{ij} (which is the synthetic for data point i due to a unit perturbation of model parameter j) is an oscillatory function of the position of the inhomogeneity and hence of the index j. This oscillatory character makes it impossible to use some interpolation scheme to compute G_{ij}. However, the phase functions ϕ_R, ϕ_L and the complex amplitudes A_R, A_L are smooth functions of the location of the inhomogeneity. This makes it possible to store these terms at selected grid points and to compute values at intermediate points by interpolation during the inversion. One could call this procedure "Filon matrix multiplication."

This procedure can be simplified even further by using the fact that the the wave numbers of the fundamental Rayleigh wave and the fundamental Love wave usually are not too different (hence $\phi_R \approx \phi_L$). If (18) is written as

$$G = Z\, e^{i\phi_R} \tag{19}$$

with

$$Z = A_R + A_L\, e^{i(\phi_L - \phi_R)}, \tag{20}$$

one only needs to store Z and ϕ_R at selected grid points.

The functions Z and ϕ_R are, in general, also a smooth function of frequency, so that the matrix only needs to be stored at certain selected frequencies. The value of the matrix elements for intermediate frequencies can also be computed by interpolation. This interpolation with respect to frequency can be performed with a simple linear interpolation. For the interpolation with respect to the location of the inhomogeneity it is better to use a quadratic scheme. The reason for this is that the phase ϕ_R has a minimum on the minor arc between the source and the receiver. It is especially at this location that accuracy is required if the isotropic approximation is used, because in that case the requirement of a small scattering angle confines the solution to the vicinity of the minor arc. A linear interpolation scheme for the horizontal coordinates is not able to reproduce such a minimum and is thus unsuitable.

In the inversions shown in paper 2 for the structure under Europe and the Mediterranean, an area of $3500\times3500\ \mathrm{km}^2$ is investigated. Storing the matrix on a 15x15 grid and interpolating in between produced accurate results. (Halving the grid distance for the interpolation did not change the solution.) In the period range from 30 s to 100 s, only 15 frequencies were sufficient to achieve an accurate interpolation with respect to frequency. (Doubling the number of frequency points for the interpolation did not change the solutions.) In this way, only 2 Mbyte of disc space was needed to store the interpolation coefficients for the matrix G.

The edges of the domain of inversion require special attention. Artificial reflections may be generated at the edge of the domain of inversion if this domain is truncated abruptly (E. Wielandt, personal communication, 1986). This problem can be circumvented by tapering the matrix G near the edges of the domain. In the inversions used in this study a linear taper was applied to G near the edges of the domain over a length of 254 km.

The theory formulated here is strictly valid only in the far field [*Snieder and Nolet*, 1987]. It can be seen from (14) that the theory becomes singular in the near field. Due to the lack of a better theory, this problem is ignored in this study. The singularity was removed by replacing the $\sin\Delta$ term in the propagator (14) by a constant ($\sin\Delta_o$), whenever $\Delta<\Delta_o$. A value of 2.7° was adopted for Δ_o.

The data fit (15) or (16) is performed in the frequency domain, whereas surface wave data are recorded in the time domain. After applying some taper these data can be transformed to the frequency domain. In case one uses the isotropic approximation a time window is needed to extract only the direct wave. In general, the data are therefore in the time domain multiplied with some nonnegative time window $w(t)$. Of course, the matrix elements, which are the spectral components of the inhomogeneity in each cell, should incorporate the effects of this time window. A multiplicative window in the time domain acts as a convolution in the frequency domain, which complicates the inversion. However, it is shown in Appendix A that if the time window $w(t)$ is nonnegative and sufficiently broad, that due to the surface wave character of the signal this filter acts in the frequency domain as a simple multiplication with $w(L/U(\omega))$. In this expression, L is the distance covered by the surface wave, and $U(\omega)$ is the group velocity of the mode under consideration.

6. WAVEFORM FITTING BY NONLINEAR OPTIMIZATION

The theory presented here establishes an inversion scheme in case a linear relation exists between the inhomogeneity and the deviation between the recorded surface waves and the synthetics for the reference model. In practice, this relation may suffer from nonlinearities. The main culprit for this effect is that small changes in the wave number are multiplied in the exponent by a large epicentral distance so that $\exp i(k+\delta k)L = (1+i\,\delta kL)\exp ikL$ may be a poor approximation.

It is therefore desirable to perform first a nonlinear inversion in order to find a smooth reference model for the Born inversion. This nonlinear inversion can be achieved by minimizing the penalty function

$$F(m) = \sum_{r,s} \int \left[u^{rs}(t) - s^{rs}(m,t)\right]^2 dt + \gamma \iint |\nabla_1 m|^2 d\Omega \quad (21)$$

with respect to the model parameters m. In this expression, $u^{rs}(t)$ is the surface wave seismogram for source s and receiver r, while $s^{rs}(t)$ is the corresponding synthetic for model m. The last term serves to select the smoothest possible solution by minimizing the horizontal gradient $|\nabla_1 m|$.

As shown by *Nolet et al.* [1986*a*], the minimization of F in (21) can be achieved efficiently using conjugate gradients. In this kind of inversion one only needs to solve the forward problem repeatedly [*Nolet et al.*, 1986*a*], and most of the computer time is spend computing the gradient of the penalty function with respect to the model parameters. It is therefore crucial to have a fast method for computing this gradient. (In this study, the forward problem is solved using the line integrals (10) in order to incorporate ray geometrical effects. Bicubic splines are useful for representing the lateral phase velocity variations because they ensure continuity of the phase velocity with its first and second derivatives. In this approach, the model parameters m are the phase velocities at some selected grid points.)

The gradient of the misfit $M(m) = \int (u(t) - s(m,t))^2 dt$ for one source receiver pair can for band limited data be estimated analytically. It is shown in Appendix B that if the synthetic consists of a sum of modes

$$S(m,\omega) = \sum_\nu S_\nu(m,\omega) = \sum_\nu A_\nu e^{i\phi_\nu} \quad (22)$$

the gradient of the misfit can be approximated by

$$\frac{\partial M}{\partial m} = -2\sum_\nu \left\{ \frac{1}{c_\nu^2} \int \frac{\partial c_\nu}{\partial m} dx\, B_1^\nu + \frac{1}{A_\nu}\frac{\partial A_\nu}{\partial m} B_2^\nu \right\} \quad (23)$$

In this expression

$$B_1^\nu = \int \dot{s}_\nu(m,t)\left[u(t) - s(m,t)\right] dt \quad (24)$$

$$B_2^\nu = \int s_\nu(m,t)\left[u(t) - s(m,t)\right] dt \quad (25)$$

Model for scattering computation.

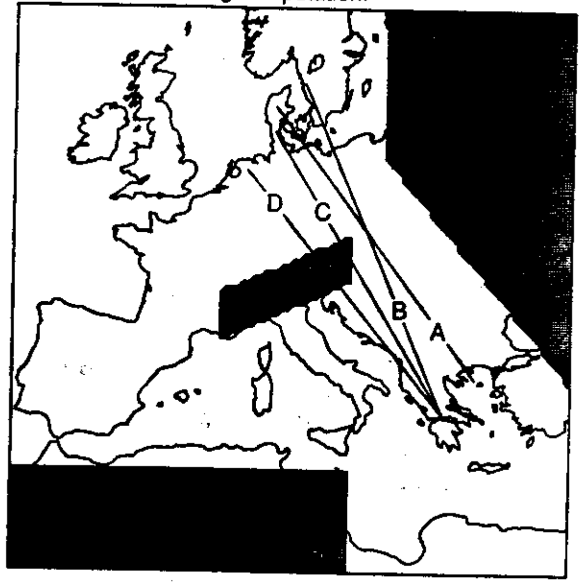

Fig. 2. Horizontal extend of the heterogeneity used in the example of the scattering computation. The inhomogeneity extends down to 170 km with $\delta\beta/\beta = 10\%$, $\delta\rho = 0$, and $\delta\lambda = \delta\mu$.

and $\int .....dx$ denotes the integral over the minor arc from the source to the receiver. The virtue of this approach is that the correlations B_1^ν and B_2^ν have to be computed only once and that the derivatives of all model parameters follow from these correlations. Note the similarity between (24) and the correlation functions used by *Lerner-Lam and Jordan* [1983] (the "bccfs") in their linear inversion of surface wave data.

7. A NUMERICAL EXAMPLE OF SCATTERED SURFACE WAVES

In order to see whether the scattering theory presented here is useful for inversion, it is instructive to study synthetic seismograms for some artificial distribution of scatterers. Figure 2 shows a fictitious distribution of scatterers which forms an extremely crude model of structures as the Alps, the Tornquist-Teisseyre zone, and the edge of north Africa. As a reference structure, the M7-model of *Nolet* [1977] is used for the density and the elastic parameters, while the attenuation of the PREM model [*Dziewonski and Anderson*, 1981] is employed. The inhomogeneity consists of a constant S velocity perturbation of 10% down to a depth of 170 km, while the density is unperturbed. Equal perturbations of the Lamé parameters are assumed. Synthetics are computed with a brute force integration of (5). In order to satisfy the criterion of linearity, only periods larger than 30 s are considered (see paper 2).

Figure 3 shows the synthetic seismogram for the laterally homogeneous reference model, the model with the inhomogeneity, and data recorded at station NE02 of the NARS network [*Dost et al.*, 1984; *Nolet et al.*, 1986*b*]. Observe the realistic looking coda in the synthetics for the model with the scatterers. Of course, one cannot speak of a fit of the recorded surface wave data for this simple minded model, but the coda in the data and in the synthetics are at least of the same nature. Given the group velocity of the surface waves, the contributions from the different scatterers can be identified by the arrival time of the surface waves. The surface waves scattered by the "Tornquist-Tesseyre zone" interfere with the later part of the

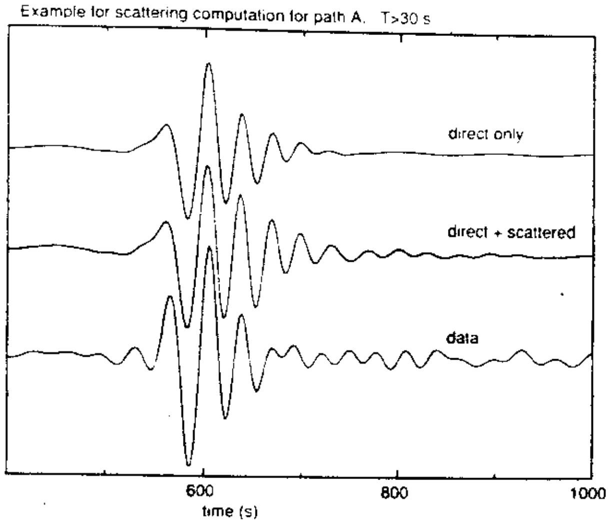

Fig. 3. Seismograms for path A of Figure 2. The top seismogram is for the laterally homogeneous reference medium, the middle seismogram is for the medium with the heterogeneity, and the bottom seismogram shows data.

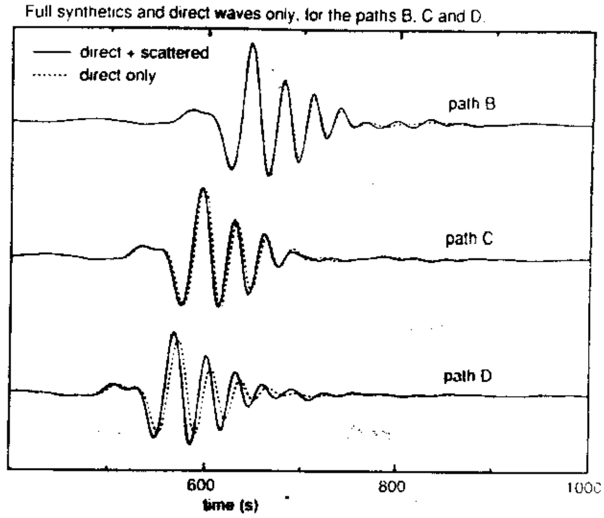

Fig. 4. Synthetic seismograms for the laterally homogeneous reference medium and the medium with the inhomogeneity for the paths B, C, and D of Figure 2.

direct wave and lead to an amplitude increase of approximately 40% of the direct surface wave train around 650 s. The surface waves scattered by the western side of the Alpine block and the diffraction by the corner of the African block constitute the surface wave coda between 750 and 950 s. The diffraction by the corner of the African block (arriving around 900 s) is rather weak because the interaction terms for the corresponding scattering angle are relatively small (see Figures 1*a* and 1*b*). However, the surface wave coda can be made arbitrarily strong by varying the strength and the location of the scatterers and by allowing shorter perids to contribute.

In Figure 4 the synthetics are shown for paths which propagate with different lengths through the central block which mimics the Alps. For path B, which does not propagate through the heterogeneity, only the coda is affected, while for the paths C and D the direct wave is substantially distorted. For path D the inhomogeneity induces both a forward time shift as well as an amplitude increase. Physically, this happens because the scattered waves arrive almost simultaneously with the direct wave (forward scattering). The resulting interference leads to a distortion of the arriving wave train. This example shows that nonsmooth structures may lead to a distortion of the direct surface wave. Interestingly, the phase shift of the direct surface wave in seismogram D coincides up to a deviation of approximately 15% with the path-averaged value of the phase velocity perturbation. This implies that in this case the phase of the direct surface wave is described well by ray theory, despite the fact that applying ray theory is strictly not justified. However, the amplitude of the surface wave is very sensitive to abrupt lateral variations of the structure.

8. INVERSION FOR A POINT SCATTERER

In order to see how the inversion for the surface wave coda operates, an example is shown where one point scatterer influences one seismogram. This point scatterer has the same depth structure as in the example of section 7, but has an effective strength of $\delta\beta/\beta \times \text{area} = 70 \times 70 \text{ km}^2$. The synthetics for the laterally homogeneous reference medium and the (synthetic) data for the medium with the scatterer are shown in the top seismograms of Figure 5. The point scatterer has generated a wave packet which arrives after the direct wave between 600 and 700 s. The Born inversion is applied to these data for a model of 100×100 cells. After three iterations the model shown in Figure 6 is produced. (The correct depth dependence of the heterogeneity is prescribed.) The corresponding synthetics are shown in the bottom seismograms of Figure 5. The "data" for this point scatterer have been fitted quite well.

The resulting model (Figure 6) bears, of course, no resemblance to the original point scatterer because it consists of an ellipsoidal band of positive and negative anomalies. With one source and one receiver it is impossible to determine the true location of the heterogeneity on this ellipse. By using more sources and

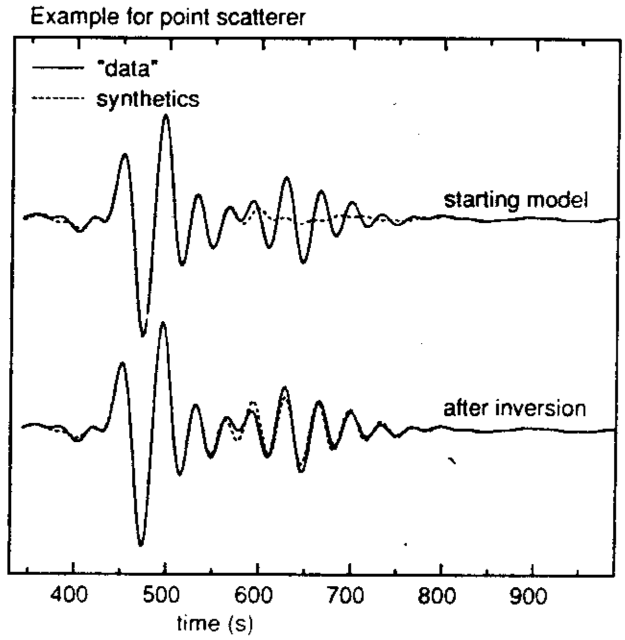

Fig. 5. Waveform fit before and after Born inversion for a synthetic seismogram generated with the point scatterer of Figure 6.

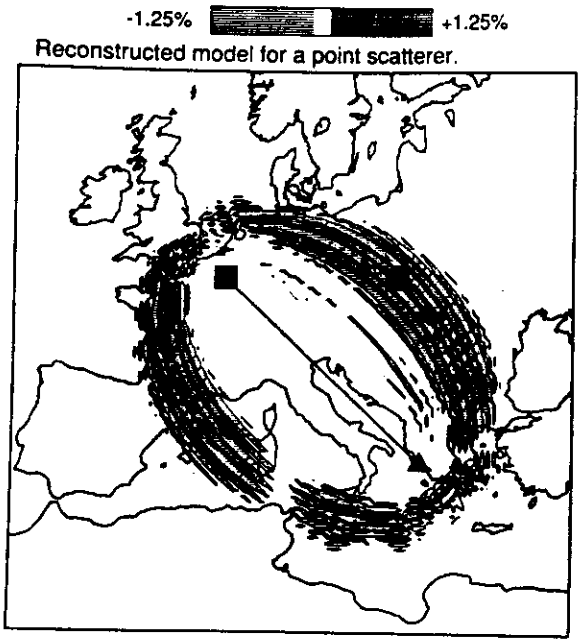

Fig. 6. Relative shear velocity perturbation ($\delta\beta/\beta$) as determined from Born inversion of the top (solid) seismogram of Figure 5. The triangle marks the source, the square marks the receiver, and the circle gives the true location of the point scatterer.

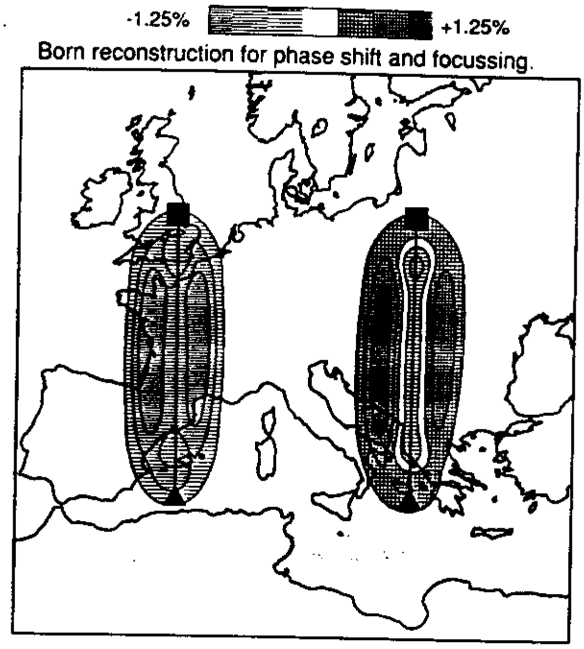

Fig. 7. Relative phase velocity perturbation ($\delta c/c$) as determined from Born inversion for ray geometrical effects. The triangles indicate the sources; the squares mark the receivers.

receivers, an image is constructed by the superposition of these ellipses.

As mentioned in section 4, the result of the first iteration of the Born inversion is proportional to $\mathbf{G}^T\mathbf{d}$, which can be interpreted as the temporal correlation between the excited wave field and the back propagated data residuals [*Snieder*, 1987*a*]. Since surface wave trains consist of oscillating wave packets, this correlation also has an oscillatory nature, which produces the alternation of positive and negative anomalies in Figure 6. The "holes" in these ellipses are caused by the nodes in the radiation pattern of the source (a double couple) and in the radiation pattern of the scatterers (the thick solid curve in the Figures 1*a* and 1*b*).

The strength of the reconstructed inhomogeneity is of the order of 1%, whereas the synthetic "data" have been computed for a point inhomogeneity of 100% with an effective area of 70×70 km^2. The reconstructed heterogeneity is spread out over a much larger area, which explains the weakened reconstructed image. Suppose the heterogeneity is spread out over zone of 2000×300km^2, which is about the right size (see Figure 6). This would lead to a weakening of the reconstructed image of 70×70 km^2/2000×300 km$^2 \approx 1\%$, which is of the order of magnitude of the reconstruction in Figure 6.

9. Inversion for Ray Geometrical Effects

In this section it is shown how the Born inversion takes ray geometrical effects such as focusing and phase shifting into account. Synthetics have been computed for the two source-receiver pairs shown in Figure 7, assuming a double-couple source for the excitation. The seismogram for the right wave path has been multiplied with 1.4, and the seismogram for the left wave path has been shifted backward in time over 4 s (which is roughly 1% of the travel time).

These seismograms have been inverted simultaneously with the Born inversion using the isotropic approximation. In this inversion a smoothness criterion is imposed because, in contrast to the scattering example of section 8, no sharp heterogeneities are needed to generate the perturbations of the wave field. The domain shown in Figure 7 consists of 100×100 cells of 35×35 km^2. The smoothing matrix that is used is given by

$$S_{i_\phi i_\theta, j_\phi j_\theta} = \alpha^{|i_\phi - j_\phi|}\,\alpha^{|i_\theta - j_\theta|} \quad \text{if} \quad |i_\phi - j_\phi| \le N \quad \text{and} \quad |i_\theta - j_\theta| \le N$$

$$S_{i_\phi i_\theta, j_\phi j_\theta} = 0 \qquad \text{elsewhere} \qquad (26)$$

where i_ϕ, i_θ, etc., denote the cell indices in the horizontal directions. In this example the values α=0.66 and N=4 are adopted.

The resulting model after three iterations is shown in Figure 7. Note that because the isotropic approximation is used, Figure 7 displays the phase velocity perturbation $\delta c/c$. (In the inversion a constant value of $\delta c/c$ over the whole frequency band is assumed.) In Figure 8 the waveform fit for the left wave path in

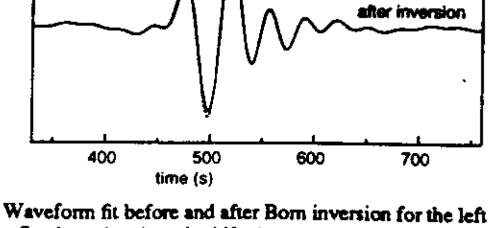

Fig. 8. Waveform fit before and after Born inversion for the left wave path in Figure 7, where the phase is shifted.

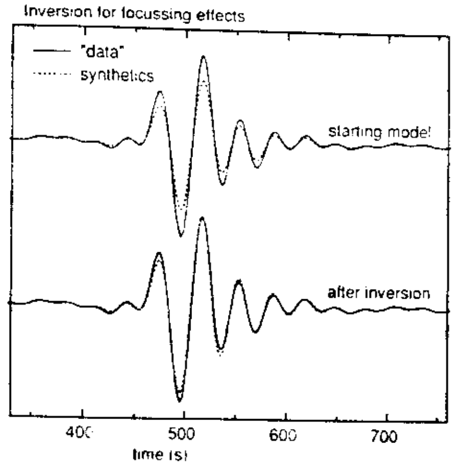

Fig. 9. Waveform fit before and after Born inversion for the right wave path in Figure 7, where the amplitude is increased.

shown. (This is the time shifted seismogram.) The phase shift is correctly taken into account. This is realized by a negative phase velocity anomaly in the first Fresnel zone of the left wave path in Figure 7. This negative phase velocity anomaly is not distributed evenly over the first Fresnel zone of the left wave path; there are phase velocity minima slightly away from the source receiver minor arc. If these minima were absent, the resulting concave transverse phase velocity profile would produce an anomalously large amplitude due to focusing. Because of the phase velocity minima adjacent to the source receiver minor arc, the transverse phase velocity profile is actually convex at the minor arc. This produces defocusing of surface wave energy, which compensates the amplitude increase due to refraction at the edge of the Fresnel zone.

The seismograms for the right wave path are shown in Figure 9. The synthetic data are 40% too strong for the laterally homogeneous reference model; this is almost completely taken care of in the inversion. Physically, this is achieved by a negative phase velocity anomaly on the source receiver line and an anomalously high phase velocity just away from this line. This phase velocity pattern leads to focusing of surface wave energy, so that the large amplitude is fitted. This confirms not only that surface wave scattering theory can account for ray geometrical effects [*Snieder*, 1987*b*], but also that these ray geometrical effects are taken care of in the Born inversion. The asymmetry of the phase velocity pattern in Figure 7 around the wave paths is due to the the asymmetry in the radiation pattern of the double-couple source.

There are approximately 10 cells between the maxima in the strips of high phase velocities for the right wave path in Figure 7. The focusing produced by this structure is achieved by the transverse curvature of the phase velocity. Increasing the cell size (which is computationally advantageous) leads to a representation of this curvature with only a few cells, which may produce unacceptable inaccuracies.

10. CONCLUSION

Large-scale inversion of the surface wave coda can in principle be performed using an iterative solver of a large system of linear equations. For this kind of inversion the depth dependence of the heterogeneity should be prescribed or be parameterized in a limited number of basis functions. Alternatively, the isotropic approximation can be used, which leads to a waveform fit of the direct surface wave due to a laterally heterogeneous phase velocity field. These phase velocities, determined for different frequency bands, can be inverted locally to a depth distribution of the heterogeneity.

The Born inversions shown in this paper are performed iteratively using LSQR. Although LSQR is originally designed for sparse matrices and the matrix for surface wave scattering is not sparse, good results are obtained in inversions of synthetic data. In practice, three iterations proved to be sufficient both for an inversion for the surface wave coda and of the direct wave. A similar conclusion was drawn by *Gauthier et al.* [1986], who used an iterative scheme for fitting waveforms in an exploration geophysics setting.

In hindsight, the success of linear waveform inversions in a few number of iterations is not so surprising. It has been argued by *Tarantola* [1984*a,b*] that the standard Kirchhoff migration methods in exploration seismics is equivalent to the first (steepest descent) step of an iterative optimization scheme. Analogously, the first step of the iterative matrix solver used here amounts to a holographic inversion [*Snieder*, 1987*a*] analogously to Kirchhoff migration. These one-step migration methods have been extremely successful in oil exploration, and there is no principal reason why a similar scheme cannot be used in global seismology. Applications of this technique to surface wave data recorded by the NARS array are shown in paper 2 [*Snieder*, this issue].

APPENDIX A: EFFECT OF THE TIME WINDOW FUNCTION ON THE SPECTRUM OF SURFACE WAVES

Suppose that a surface wave seismogram $s(t)$ is multiplied with some nonnegative window function $w(t)$ to give a windowed seismogram $f(t)$

$$f(t) = w(t)s(t) \tag{A1}$$

In the frequency domain the application of this window leads to a convolution

$$F(\omega) = \int W(\omega')S(\omega-\omega')\, d\omega' \tag{A2}$$

Since $w(t)$ is nonnegative, $|W(\omega)|$ attains its maximum for ω=0; this can be seen by making the following estimates:

$$|W(\omega)| = |\int w(t)e^{i\omega t} dt| \le \int |w(t)e^{i\omega t}| dt$$
$$= \int w(t)dt = |W(\omega{=}0)| \tag{A3}$$

If the time window has a length T in the time domain, its frequency spectrum will have a width of the order π/T in the frequency domain. From this we conclude that long nonnegative time windows have a spectrum that peaks around ω=0.

Now assume that the surface wave spectrum consists of one mode (extensions to multimode signals are straightforward):

$$S(\omega) = A(\omega)e^{ik(\omega)L} \tag{A4}$$

where L is the epicentral distance. Substituting in (A2) gives

$$F(\omega) = \int W(\omega')A(\omega-\omega')e^{ik(\omega-\omega')L}\, d\omega' \tag{A5}$$

$W(\omega)$ is a function peaked around ω=0, so that the main contribution to the ω' integral comes from the point ω'=0. Usually, the complex amplitude $A(\omega)$ is a smooth function of frequency, so that one can approximate for small ω'

$$A(\omega-\omega') \approx A(\omega) \tag{A6}$$

The phase term can be analyzed with a simple Taylor expansion

$$k(\omega-\omega')L \approx k(\omega)L - \frac{L\omega'}{U(\omega)} \quad \text{(A7)}$$

where $U(\omega)$ is the group velocity of the surface wave mode. Inserting (A6) and (A7) in (A5) gives

$$F(\omega) \approx A(\omega)e^{ik(\omega)L} \int W(\omega')e^{-iL\omega'/U(\omega)}\, d\omega' \quad \text{(A8)}$$

With (A4) and the definition of the Fourier transform this leads to

$$F(\omega) \approx S(\omega)\, w(L/U(\omega)) \quad \text{(A9)}$$

APPENDIX B: ANALYTICAL ESTIMATION OF THE GRADIENT $\partial M/\partial m$

The misfit between the data $d(t)$ and the surface wave synthetics $s(m,t)$ for model m is in the L_2 norm defined by

$$M \equiv \int |d(t) - s(m,t)|^2 dt \quad \text{(B1)}$$

Using Parseval's theorem [*Butkov*, 1968], the misfit has the same form in the frequency domain

$$M = \int |D(\omega) - S(m,\omega)|^2 d\omega \quad \text{(B2)}$$

In general, the model m consists of many parameters. The derivative of the misfit with respect to one of these parameters is

$$\frac{\partial M}{\partial m} = -2\,\mathrm{Re}\left\{\int \frac{\partial S(m,\omega)}{\partial m}(D^*(\omega)-S^*(m,\omega))\, d\omega\right\} \quad \text{(B3)}$$

Let the surface wave seismogram be given by a superposition of modes ν with complex amplitude A_ν and phase ϕ_ν

$$S(m,\omega) = \sum_\nu S_\nu(m,\omega) = \sum_\nu A_\nu(m,\omega)e^{i\phi_\nu(m,\omega)} \quad \text{(B4)}$$

so that

$$\frac{\partial S}{\partial m} = \sum_\nu \left[\frac{1}{A_\nu}\frac{\partial A_\nu}{\partial m} + i\frac{\partial \phi_\nu}{\partial m}\right] S_\nu \quad \text{(B5)}$$

According to equation (10), the phase of the surface waves is in a laterally heterogeneous medium

$$\phi(\omega) = \int_0^L k(\omega,x)\, dx \quad \text{(B6)}$$

where $k(\omega,x)$ is the local wave number. Differentiation with respect to the model parameter m gives

$$\frac{\partial \phi}{\partial m} = \int_0^L \frac{\partial k}{\partial m}\, dx = -\frac{\omega}{c^2}\int_0^L \frac{\partial c}{\partial m}\, dx \quad \text{(B7)}$$

Inserting this in (B5) gives

$$\frac{\partial M}{\partial m} = -2\,\mathrm{Re}\left\{\sum_\nu \int \frac{1}{A_\nu}\frac{\partial A_\nu}{\partial m} S_\nu(m,\omega)\left[D^*(\omega)-S^*(m,\omega)\right] d\omega\right\}$$

$$+2\,\mathrm{Re}\left\{\sum_\nu \int \frac{i\omega}{c_\nu^2}\left[\int_0^L \frac{\partial c_\nu}{\partial m}dx\right] S_\nu(m,\omega)\left[D^*(\omega)-S^*(m,\omega)\right] d\omega\right\} \quad \text{(B8)}$$

When one is attempting to find phase velocities by nonlinear optimization, one will usually work with band passed data for which $c(\omega)$ can be assumed to be independent of frequency. In that case, the phase velocity term and the amplitude term can be taken out of the frequency integral. Applying Parseval's theorem once more to the resulting expression gives

$$\frac{\partial M}{\partial m} = -2\sum_\nu \frac{1}{c_\nu^2}\left[\int \frac{\partial c_\nu}{\partial m}dx\right]\int \dot{s}_\nu(m,t)\left[d(t)-s(m,t)\right]dt$$

$$-2\sum_\nu \frac{1}{A_\nu}\frac{\partial A_\nu}{\partial m}\int s_\nu(m,t)\left[d(t)-s(m,t)\right]dt \quad \text{(B9)}$$

which proves equation (23).

REFERENCES

Backus, G.E., Geographical interpretation of measurements of average phase velocities over great circular and great semi circular paths, *Bull. Seismol. Soc. Am.*, *54*, 571–610, 1964.

Berkhout, A.J., *Seismic Migration, Imaging of Acoustic Energy by Wave Field Extrapolation, B, Practical Aspects*, Elsevier, Amsterdam, 1984.

Bungum, H., and J. Capon, Coda pattern and multipathing propagation of Rayleigh waves at NORSAR, *Phys. Earth Planet. Inter.*, *9*, 111–127, 1974.

Butkov, E., *Mathematical Physics*, Addison-Wesley, Reading, Mass., 1968.

Calcagnile, G., and R. Scarpa, Deep structure of the European-Mediterranean area from seismological data, *Tectonophysics*, *118*, 93–111, 1985.

Dahlen, F.A., The spectra of unresolved split normal mode multiplets, *Geophys. J. R. Astron. Soc.*, *58*, 1–33, 1979.

Dost, B., A. van Wettum, and G. Nolet, The NARS array, *Geol. Mijnbouw*, *63*, 381–386, 1984.

Dziewonski, A.M., and D.L. Anderson, Preliminary reference Earth model, *Phys. Earth Planet. Inter.*, *25*, 297–356, 1981.

Gauthier, O., J. Virieux, and A. Tarantola, Two-dimensional nonlinear inversion of seismic waveforms: Numerical results, *Geophysics*, *51*, 1387–1403, 1986.

Gilbert, F., and A. Dziewonski, An application of normal mode theory to the retrieval of structural parameters and source mechanisms from seismic spectra, *Philos. Trans. R. Soc. London, Ser. A 278*, 187–269, 1975.

Jordan, T.H., A procedure for estimating lateral variations from low frequency eigenspectra data, *Geophys. J. R. Astron. Soc.*, *52*, 441–455, 1978.

Lerner-Lam, A.L., and T.J. Jordan, Earth structure from fundamental and higher-mode waveform analysis, *Geophys. J. R. Astron. Soc.*, *75*, 759–797, 1983.

Levshin, A., and K.A. Berteussen, Anomalous propagation of surface waves in the Barentz Sea as inferred from NORSAR recordings, *Geophys. J. R. Astron. Soc.*, *56*, 97–118, 1979.

Nolet, G., The upper mantle under Western-Europe inferred from the dispersion of Rayleigh wave modes, *J. Geophys.*, *43*, 265–285, 1977.

Nolet, G., Linearized inversion of (teleseismic) data, in *The Solution of the Inverse Problem in Geophysical Interpretation*, edited by R. Cassinis, pp. 9–38, Plenum, New York, 1981.

Nolet, G., J. van Trier, and R. Huisman, A formalism for nonlinear inversion of seismic surface waves, *Geophys. Res. Lett.*, *13*, 26–29, 1986*a*.

Nolet, G., B. Dost, and H. Paulssen, Intermediate wavelength seismology and the NARS experiment, *Ann. Geophys.*, *B4*, 305–314, 1986*b*.

Paige, C.G., and M.A. Saunders, LSQR: An algorithm for sparse linear equations and sparse least squares, *ACM Trans. Math. Software*, *8*, 43–71, 1982*a*.

Paige, C.G., and M.A. Saunders, LSQR: Sparse linear equations and least squares problems, *ACM Trans. Math. Software*, *8*, 195–209, 1982*b*.

Panza, G.F., S. Mueller, and G. Calcagnile, The gross features of the lithosphere-asthenosphere system from seismic surface waves and body waves, *Pure Appl. Geophys.*, *118*, 1209–1213, 1980.

Romanowicz, B., Multiplet-multiplet coupling due to lateral heterogeneity: Asymptotic effects on the amplitude and frequency of the Earth's normal modes, *Geophys. J. R. Astron. Soc.*, *90*, 75–100, 1987.

Romanowicz, B., and R. Snieder, A new formalism for the effect of lateral heterogeneity on normal modes and surface waves, II, General anisotropic perturbations, *Geophys. J. R. Astron. Soc.*, *93*, 91–100, 1988.

Snieder, R., 3D Linearized scattering of surface waves and a formalism for surface wave holography, *Geophys. J. R. Astron. Soc.*, *84*, 581–605, 1986*a*.

Snieder, R., The influence of topography on the propagation and scattering of surface waves, *Phys. Earth Planet. Inter.*, *44*, 226–241, 1986*b*.

Snieder, R., Surface wave holography, in *Seismic Tomography, With Applications in Global Seismology and Exploration Geophysics*, edited by G. Nolet, pp. 323–337, D. Reidel, Hingham, Mass., 1987*a*.

Snieder, R., On the connection between ray theory and scattering theory for surface waves, in *Mathematical Geophysics, A Survey of Recent Developments in Seismology and Geodynamics*, edited by N.J., Vlaar, G., Nolet, M.J.R., Wortel, S.A.P.L. and Cloetingh, pp. 77–83, D. Reidel, Hingham, Mass., 1987*b*.

Snieder, R., Large-scale waveform inversions of surface waves for lateral heterogeneity, 2, Application to surface waves in Europe and the Mediterranean, *J. Geophys. Res., this issue*, 1988.

Snieder, R., and G. Nolet, Linearized scattering of surface waves on a spherical Earth, *J. Geophys.*, *61*, 55–63, 1987.

Snieder, R., and B. Romanowicz, A new formalism for the effect of lateral heterogeneity on normal modes and surface waves, I, Isotropic perturbations, perturbations of interfaces and gravitational perturbations, *Geophys. J. R. Astron. Soc.*, *92*, 207–222, 1988.

Spakman, W., and G. Nolet, Imaging algorithms, accuracy and resolution in delay time tomography, in *Mathematical Geophysics, A Survey of Recent Developments in Seismology and Geodynamics*, edited by N.J., Vlaar, G., Nolet, M.J.R., Wortel, S.A.P.L. and Cloetingh, pp. 155–187, D. Reidel, Hingham, Mass., 1987.

Tanimoto, T., The three-dimensional shear wave velocity structure in the mantle by overtone waveform inversion, I, Radial seismogram inversion, *Geophys. J. R. Astron. Soc.*, *89*, 713–740, 1987.

Tarantola, A., Inversion of seismic reflection data in the acoustic approximation, *Geophysics*, *49*, 1259–1266, 1984*a*.

Tarantola, A., Linearized inversion of seismic reflection data, *Geophys. Prospect.*, *32*, 998–1015, 1984*b*.

Tarantola, A., and B. Valette, Generalized nonlinear inverse problems solved using the least squares criterion, *Rev. Geophys.*, *20*, 219–232, 1982.

Van der Sluis, A., and H.A. Van der Vorst, Numerical solution of large, sparse linear algebraic systems arising from tomographic problems, in *Seismic Tomography, With Applications in Global Seismology and Exploration Geophysics*, edited by G. Nolet, pp. 49–83, D. Reidel, Hingam, Mass., 1987.

Woodhouse, J.H., and Y.K. Wong, Amplitude, phase and path anomalies of mantle waves, *Geophys. J. R. Astron. Soc.*, *87*, 753–774, 1986.

Yomogida, K., and K. Aki, Amplitude and phase data inversion for phase velocity anomalies in the Pacific Ocean basin, *Geophys. J. R. Astron. Soc.*, *88*, 161–204, 1987.

R. Snieder, Department of Theoretical Geophysics, University of Utrecht, P.O. Box 80.021, 3508 TA Utrecht, The Netherlands.

(Received October 13, 1987;
revised April 21, 1988;
accepted April 25, 1988.)